

Sputtering of parent-like ions from large organic adsorbates on metals under keV ion bombardment

A. Delcorte *, P. Bertrand

*Unité de Physico-Chimie et de Physique des Matériaux, Université Catholique de Louvain, 1 pl. Croix du Sud,
B-1348 Louvain-la-Neuve, Belgium*

Received 24 January 1998; accepted for publication 12 May 1998

Abstract

Thin films of hydrocarbon molecules, unsaturated fatty acid and low molecular weight polystyrene deposited on different metal substrates (silver, copper and gold) were bombarded by 15 keV Ga ions and the secondary ions were mass- and energy-analysed by means of a time-of-flight secondary ion mass spectrometer. The samples were studied in order to evidence the effects of different substrates and coverages on the emission of the parent and cationised molecular ions, and to gain a better understanding of the large molecular ion emission processes. Ion beam degradation studies were realised for fundamental purposes too. In general, the kinetic energy distributions of metal-cationised molecules are broad in comparison with those of the parent ions, and of the smaller polystyrene fingerprint ions. In addition, the velocity distributions of the parent ions and of the metal-cationised molecules are similar. Parent ions of aromatic molecules are, on average, more energetic than those of aliphatic molecules. In the case of metal-cationised molecules, the three hypotheses of emission of a preformed complex, recombination in the seldedge and metastable decay of larger aggregates are critically reviewed in comparison with the experimental data. The recombination hypothesis cannot account for the whole set of observations. On the other hand, the very different evolutions of the parent ions and of the metal-cationised molecules in the degradation experiments cannot be explained solely in the frame of metastable decay reactions, although the kinetic energy measurements show that a significant fraction of the parent-like ions are produced in the vacuum. The augmentation of the secondary ion kinetic energy with increasing molecule size for triacontane monomers and dimers, and for silver-cationised polystyrene oligomers, is in disagreement with the sputtering by a single cascade atom, too. Finally, the discussion outlines the conditions that must be satisfied to model the experimental observations and proposes a view of the sputtering of these large molecular cations based on multiple collision processes and possible subsequent dissociation in the vacuum. © 1998 Published by Elsevier Science B.V. All rights reserved.

Keywords: Cationisation; Ion emission; Matrix effects; Metastable decay; Polystyrene; Secondary ion mass spectrometry (SIMS); Silver; Sputtering

1. Introduction

The mechanisms of secondary ion emission from organic materials bombarded by keV ions are not very well known yet. In particular, the emission of

large molecular ions from polymer surfaces is difficult to understand on the basis of simple mechanistic arguments involving single atom collisions [1–4]. In order to achieve high yields of large molecular ions in SIMS of organic materials and low molecular weight polymers and to have insight into the fragmentation processes of polymers, the cationisation of sputtered particles by complex-

* Corresponding author. Tel: +32 10 473582;
Fax: +32 10 473452; e-mail: delcorte@pcpm.ucl.ac.be

ation with substrate atoms is often used [5–13]. It has been firstly reported by Grade et al. in a short communication in 1977 [5]. In most cases, the metal (Me) is thought to bring the positive charge to the neutral organic molecule (M), resulting in the formation of an organometallic complex ion of the kind $(M+Me)^+$. In fact, the way by which such complexes are formed is not straightforward. In general, three hypotheses are considered [14]: (i) the complex is formed at the surface and is sputtered without fragmentation or recombination (precursor model) [15–24]; (ii) the complex ion is formed in the selvedge by the recombination of a neutral molecule with a metal ion [25,26]; and (iii) the complex ion is formed from the metastable decay of larger M_xMe_y clusters [27] (the same explanation was previously proposed for analytes dissolved in a matrix [28,29]). It is interesting to note that negatively charged organometallic complexes have been observed too, depending on the type of metallic substrate chosen [23,24,27]. The roles of the binding energy with the metal substrate and of the metal reactivity on the cationisation efficiency have been highlighted too [14]. On the other hand, a lot of examples from the literature show that the cationisation is favoured for unsaturated hydrocarbons in comparison with saturated ones [30–32]. The interaction between silver (copper, gold) and unsaturated hydrocarbons has been explained by the efficient overlap between the π -orbitals of the hydrocarbon and the energetically accessible d-orbitals of the metal atom, resulting in the formation of “ π -complexes”. This form of metal–carbon interaction is specific to transition metals [33]. The charge transfer increases with silver (copper, gold) cations instead of atoms, due to their higher acceptor strength, which may explain the stability of the organometallic formed ions.

The most common procedure for sample preparation in silver cationisation experiments consists in depositing a droplet of a very dilute analyte solution on a clean silver surface. UHV deposition of the analyte has been used too, in the case of amino-acids [16]. The substrate can be a silver foil etched in nitric acid [7,8], or an Ag-metallised support [32,34]. In addition, silver cationisation has been reported for metallised oligomer coatings

[34,35], as well as for mixtures of PS oligomers, silver trifluoroacetate salt and dihydroxybenzoic acid deposited on various substrates from a THF solution, following the sample preparation procedure used in time-of-flight matrix assisted laser desorption ionisation (ToF-MALDI) [36]. In both cases, the presence of large silver aggregates which might be covered by the low molecular weight polystyrene would not discard an emission process based on the development of the collision cascade in the large silver clusters. In the case of polymers, the cationisation method has been extensively used to obtain the molecular weight distribution of the polymer chains, below 12 000 Da [8]. The differences observed with more classical determinations of the number average molecular weight M_n (around 10% error) have been attributed to a mass-dependent fragmentation of the macrochains [8,37], which must somehow be related to the size of the area excited by the primary ion impact. Another important parameter is the detection efficiency which decreases drastically at such high masses.

In addition to the determination of the secondary ion yields, the analysis of the kinetic energy distributions (KEDs) of the molecular secondary ions observed in the spectra of organic compounds and polymers has been initiated recently in our laboratory, in order to gain a deeper understanding of the ion sputtering from organic surfaces [38–42,44,46]. Indeed, the KED of the particles sputtered from solid surfaces provides important information concerning the mechanism of emission itself [47]. However, when dealing with the KED of secondary ions instead of neutrals, one must be aware of the possible energy dependence of the ionisation process. Nevertheless, the interpretation of the KED of molecular fragment ions sputtered from tricosenoic acid Langmuir–Blodgett layers gave indications about the fragmentation occurring in the surface region, and highlighted the predominant effect of the chemical structure of the bombarded species [38,39]. The influence of the ionisation was ruled out by comparing the distributions of the negative and positive C_xH_y secondary ions. This has been confirmed with polymer samples. For instance, the very narrow KED of the polymer fingerprint ions, e.g. $C_6H_4^+$ and

$C_6H_4CO^+$ sputtered from poly(ethylene terephthalate) [40], $C_xH_{2x}^+$ sputtered from poly(isobutylene) [44], and $C_xH_x^+$ sputtered from poly(styrene) [41,42,44], indicated soft emission mechanisms. In contrast, the broader KED of more fragmented or reorganised ions involved more violent emission processes. From these observations, it could be deduced that atomic or little fragment ions which have lost the memory of the polymer structure were produced in the region of the primary ion impact, where the deposited energy is high, whereas the polymer characteristic ions were mainly produced at some distance from the primary impact point, where the deposited energy is much lower. Very similar effects have been observed by Papaléo et al. with heavy MeV primary ions [48,49] and by Zubarev et al. with keV primary ions [50]. In addition, the ion fragments resulting from unimolecular dissociation of their metastable parents in the linear part of the spectrometer can be observed in the energy spectrum of the secondary ion too [41,42,44,46,51]. When they dissociate, the parents share their kinetic energy between the neutral and ion fragments in a proportion depending on the respective masses of these fragments. Consequently, the daughter ions originating from the dissociation process will be detected with a kinetic energy $E_{acc} - \Delta E_{neutral}$, lower than the kinetic energy of identical ions directly emitted from the surface. For short lifetimes, typically in the range 10^{-9} – 10^{-7} s, the dissociation reaction occurs in the acceleration section of the ToF spectrometer. Then, the metastable ions decompose before being completely accelerated (3 kV). These daughter ions having a kinetic energy deficit constitute a “negative energy” tail in the KEDs.

On the other hand, Briggs et al. and Leggett et al. have shown that a fundamental information about the molecular ion emission processes could be deduced from ion beam degradation measurements [52,53]. This method has been used in our group too, showing for instance that the evolution of the secondary ion yields could be directly related to the physico-chemical modifications of the surface, and revealing which ions were the most characteristic of a given chemical structure [54]. Possible parent ions in some particular metastable

decay reactions could be identified by this way too [44].

In this paper, the analysis of the large molecular ion KEDs and of their degradation under ion beam bombardment will allow us to revisit the different models proposed for the emission of parent ions and metal-cationised molecules.

For simplicity, the simultaneous emission of a molecule with an adjacent metal atom of the substrate in the same event will be considered as the emission of a “preformed complex” or “precursor”, even if the metal atom is not really bound to the molecule prior to emission, which is slightly different to the conventional use of the term “precursor” proposed by Benninghoven [15].

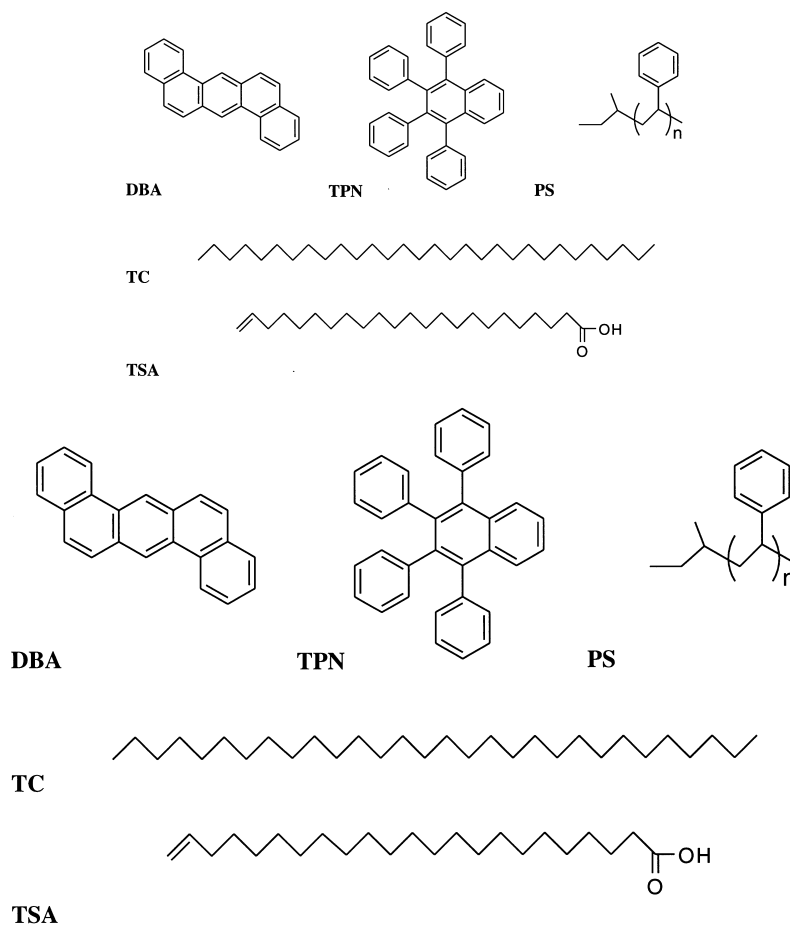
2. Experimental

2.1. Samples

The triacontane (TC: $C_{30}H_{62}$, formula weight (FW)=422.8), 1,2:5,6-dibenzanthracene (DBA: $C_{22}H_{14}$, FW=278.35) and 1,2,3,4-tetraphenyl-naphthalene (TPN: $C_{10}H_4(C_6H_5)_4$, FW 432.57) were purchased from Aldrich Chemie (Scheme 1). They were dissolved respectively in benzene (TC and TPN) and acetone (DBA).

The two polystyrene samples used for this study were: (i) PS700 (number average molecular weight, $M_n=700$; weight average molecular weight, $M_w=790$) purchased from Scientific Polymer Products Inc., and (ii) PS1100 ($M_n=1100$; $M_w=2200$) synthesised by I. Fallais at the University of Liège [36]. They were used to observe the KED of Ag-cationised oligomers. The polymers were dissolved in toluene.

The concentration of the solutions was approximately 1 mg ml^{-1} ($\sim 10^{-2} \text{ mol l}^{-1}$ for PS and $\sim 2\text{--}3 \times 10^{-3} \text{ mol l}^{-1}$ for TC, TPN and DBA). In the case of TC and TPN, additional solutions of 0.1 and 10 mg ml^{-1} were realised. For each sample, a droplet of the corresponding solution was deposited on a clean silver and/or copper substrate (TC). For comparison purpose, TC and TPN were also cast on silver- and gold-metallised silicon wafers, and on clean silicon wafers. Prior to casting, the silver and copper foils, and the silver- and



Scheme 1.

gold-metallised silicon wafers were etched in a solution of nitric acid (25% HNO_3) for 20 s and subsequently rinsed in ultra-pure water (millipore), isopropanol and hexane. XPS measurements realised after etching indicated that the atomic ratios Cu:O and Ag:O were close to 1:1 and 3:1, respectively.

The preparation of the LB films of tricosenoic acid on gold (TSA: $\text{C}_{22}\text{H}_{43}\text{COOH}$) has been described elsewhere [38,39].

2.2. ToF-SIMS

The SIMS analyses and the KED measurements were performed with a Phi-Evans TRIFT[®] spec-

trometer using a pulsed Ga^+ beam (FEI 83-2 LI source with 15 keV energy; 800 pA DC current; 24 ns pulse width bunched down to 1.2 ns; 5 kHz repetition rate) [55]. The angle between the gallium source and the spectrometer axis (perpendicular to the surface) was 35° . For routine analysis, the primary beam was rastered over a 0.017 mm^2 area and 300 s acquisitions were realised in the mass range $0 \leq m/z \leq 5000$, corresponding to a primary ion fluence (F) of $1.05 \times 10^{12} \text{ ions cm}^{-2}$. For polymer surface degradation studies, continuous bombardments on a larger area (0.036 mm^2) with the same Ga^+ source were alternated with routine ToF-SIMS analysis periods [54], in order to reach a maximum fluence of $10^{16} \text{ ions cm}^{-2}$. Images were

recorded on 256×256 pixels by scanning the 15 keV beam over a 0.036 mm^2 area for 240 s (mass range $0 \leq m/z \leq 1000$), corresponding to a primary ion fluence $F = 8.8 \times 10^{11} \text{ ions cm}^{-2}$.

The KED measurements have been described elsewhere [38,39,41,42]. During the secondary ions extraction periods, a $(3000 - \Delta) \text{ V}$ potential was applied to the sample where Δ is adjustable in order to acquire a selected part of the KED. The departing secondary ions were accelerated between the sample and the extraction plate (grounded entrance of the first Einzel lens) and focused before to enter the field free drift region. They were afterwards deflected 270° by three hemispherical electrostatic analysers (ESA) before reaching the detector. At the crossover following the first ESA (at 90° with respect to the spectrometer axis), they were energy selected by a slit of fixed width ($100 \mu\text{m}$ corresponding to a passband of 1.5 eV). Thus, the detected part of the KED corresponds to the mean energy $(\Delta - C) \text{ eV}$, where C is a constant. The acquisition of mass spectra for different sample voltages allowed the collection of a complete KED, a 1 V increase of the sample potential corresponding to a 1 eV decrease in the KED. An alternative way to record the KED was to keep the sample voltage at a fixed nominal value (3 kV) and to shift the energy slit perpendicularly to the beam in order to accept different regions of the KED. The spatial distribution was then converted into an energy distribution owing to an empirical equation derived from the simulation of the ion trajectories [56]. To calibrate the zero of the energy scale, the tangent to the increasing part of the KED of atomic substrate ions (Ag^+) was extrapolated to zero intensity. The corrected value of the sample voltage, giving the initial kinetic energy of the secondary ions, is called “apparent kinetic energy” in the following.

The parameters used for the analyses allowed to keep the total ion fluence below $10^{13} \text{ ions cm}^{-2}$ for a number of mass spectra covering different secondary ion energy windows, which is reasonable in comparison with the static limit for most of the studied samples [54]. However, in the case of TC, which exhibits a very high damage cross-section (see the results section), the intensities obtained during the KED measurements have been

corrected by the degradation law measured for the corresponding ions.

3. Results

3.1. SI mass spectra

3.1.1. Triacontane

The positive mass spectrum of TC shown in Fig. 1 exhibits two large Ag peaks at $m/z = 107$ and 109. In the low mass range, the dominant peaks correspond to $\text{C}_x\text{H}_{2x-1}$ and $\text{C}_x\text{H}_{2x+1}$ fragment ions, which are easily explained by the chemical structure of the TC molecule. The ions observed in the higher mass range are listed in Table 1. Around the molecule mass, the dominant peaks are $(\text{M}-2\text{H})^+$ and $(\text{M}-4\text{H})^+$. This lack of hydrogen with respect to the precursor is common for saturated hydrocarbon molecules [35,57]. This indicates that the formation of a fully saturated parent ion is not favoured. The series of peaks in the range $520 < m/z < 535$ is dominated by the ions $(\text{M}-2\text{H} + {}^{107}\text{Ag})^+$ and $(\text{M}-2\text{H} + {}^{109}\text{Ag})^+$. A weak contribution of $(\text{M} + {}^{109}\text{Ag})^+$ is observed at $m/z = 531$. It is interesting to note that the intensity of the Ag-cationised molecules is much stronger than

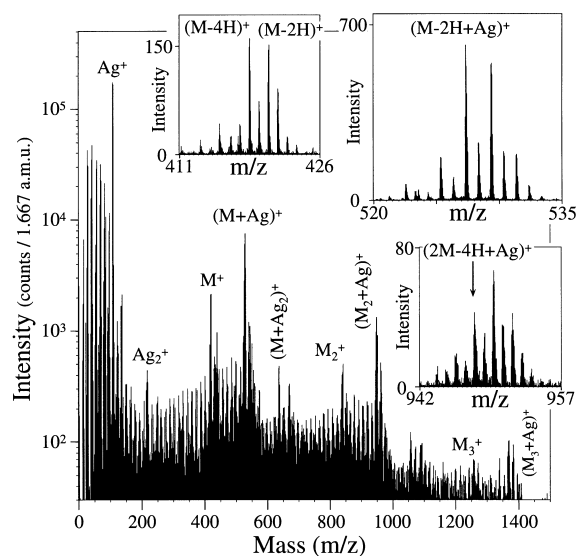


Fig. 1. Positive SI mass spectrum of TC cast on a silver foil. Insets: the SI intensity is indicated in counts/0.017 Da.

Table 1
Organic and organometallic molecular ions observed in the SI mass spectra of organic molecules cast on metal substrates

Samples	Molecular ions	$I(M+Me)/I(M)$	$I(M+Me)/I(Me)$
TC/Ag	+ (M-2H) ⁺ ; (2M-4H) ⁺ ; M ₃ ⁺ ; (M-2H+Ag) ⁺ ; (2M-4H+Ag) ⁺ ; (M ₃ +Ag) ⁺ ; (M ₄ +Ag) ⁺ ; (M-H+Ag ₂) ⁺ ; (2M-3H+Ag ₂) ⁺	4	0.05
TC/Cu	+ (M-2H) ⁺ ; (2M-4H) ⁺ ; (M-2H+Cu) ⁺ ; (2M-4H+Cu) ⁺ ; (M ₃ +Cu) ⁺ ; (M-H+Cu ₂) ⁺	7	0.007
TC/Au	+ (M-2H) ⁺ ; (2M-4H) ⁺ ; (M-2H+Au) ⁺ ; (2M-4H+Au) ⁺ ; (M ₃ +Au) ⁺ ; (M-H+Au ₂) ⁺	1.2	0.05
TC/Au	- (M+Au) ⁻	-	0.01
TPN/Ag	+ M ⁺ ; (M+Ag) ⁺ ; (2M+Ag) ⁺	2	0.6
TPN/Au	+ M ⁺ ; M ₂ ⁺ ; (M+Au) ⁺ ; (M ₂ +Au) ⁺ ; (M ₃ +Au) ⁺	1.1	50
TPN/Au	- (M-H) ⁻ ; (M+H) ⁻ ; (M+Au) ⁻	0.15	0.008
DBA/Ag	+ M ⁺ ; (M+Ag) ⁺	0.32	0.008
TSA/Au	+ (M-OH) ⁺ ; (M+H) ⁺ ; (2M-H ₂ O-OH) ⁺ ; (2M-OH) ⁺ ; (M+Au) ⁺ ; (M+H+2Au) ⁺	9	0.5
TSA/Au	- (M-H) ⁻ ; (2M-H) ⁻ ; (M+Au) ⁻ ; (M-H+2Au) ⁻	0.07	0.06
PS1100/Ag	+ (M+Ag) ⁺	-	0.04

the one of the molecules themselves: the ratio $I(M-2H+Ag^+)/I(M-2H^+)$ is greater than 4. At $m/z=635$, one can observe a group of peaks due to $(M-H+2Ag)^+$. Dimers, trimers and their cationised homologues are clearly visible around $m/z=840$, 1260 and 950, and 1370, respectively. Even cationised quadrimers are present with a weak intensity at $m/z=1790$. Parent or large molecular ions are not observed in the negative spectrum of TC. Only small unsaturated hydrocarbon fragments and very weak peaks corresponding to the Ag isotopes can be evidenced.

A very similar series of molecular cations is observed when triacontane is cast on copper instead of silver: $(M-2H)^+$ at $m/z=420$; $(M-2H+^{63}Cu)^+$ and $(M-2H+^{65}Cu)^+$ at $m/z=483$ and 485; $(M-H+2Cu)^+$ around $m/z=549$; dimers and cationised dimers around $m/z=840$ and 920. Generally, the intensity of large molecular ions is weaker in the case of copper substrate. In particular, the presence of trimers and cationised quadrimers is unclear.

Similar ions are also detected when TC is cast on a gold substrate (Table 1). Note that the ratio $I(M+Me^+)/I(Me^+)$ is the same for silver and gold supports (5%), whereas it is one order of magnitude lower for copper substrate. For TC deposited on gold, negative organometallic ions are detected too (Fig. 2). The most intense is

$(M+Au)^-$, followed by $(M-2H+Au)^-$ (three times weaker). This demonstrates that the systematic dehydrogenation observed in the positive TC spectra is not an effect of degradation, but rather a chemical effect related to the stability of the parent ion.

In contrast with copper, silver and gold substrates, triacontane cast on silicon shows the monomer, dimer and even trimer ions, but no $(M-2H+Si)^+$ complex, although Si^+ secondary ions constitute an intense peak in the mass spectrum (Fig. 3).

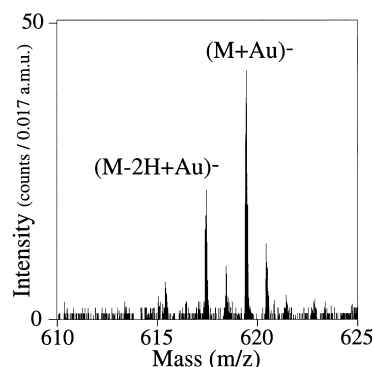


Fig. 2. Partial negative SI mass spectrum of TC cast on a gold-metallised silicon wafer. Region of the organometallic parent-like ion $(M+Au)^-$.

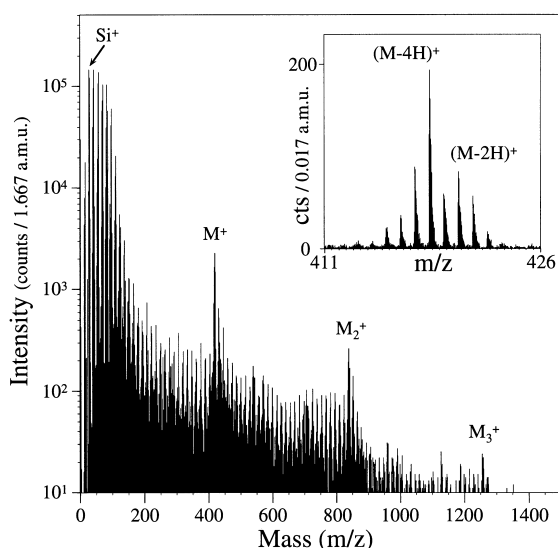


Fig. 3. Positive SI mass spectrum of TC cast on a silicon wafer.

3.1.2. Tetraphenylanthracene

In the positive ion mass spectrum of TPN (Fig. 4), the dominant peaks above $m/z=200$ are due to M^+ ($m/z=432$), $(M+Ag)^+$ ($m/z=539$ and 541) and $(2M+Ag)^+$ ($m/z=971$ and 973). Ions with two silver atoms, molecule dimers and trimers are weak or absent. The most intense fragment ion series is in the region $250 < m/z < 400$ and corresponds to polycyclic aromatic ions. In the fingerprint region, (poly)cyclic ions also show significant intensities ($m/z=77, 91, 115, 128, 152, 165, 178, 189, \dots$). The ratio $I(M+Me^+)/I(M^+)$ is close to two for TPN. Remarkably, the ratio $I(M+Me^+)/I(Me^+)$ is equal to 0.6 (Table 1), showing the efficiency of the organometallic ion production mechanism.

For TPN cast on gold, additional molecular ions are detected (Table 1), in particular M_2^+ and $(M_3+Au)^+$. It is striking to see that the signal of the gold-cationised molecule is 50 times more intense than the gold signal itself. In the negative mode, parent and organometallic ions are present too, and the gold signal is much more intense. These observations are in favour of an important chemical effect on the nature and relative fractions of the detected ions, in agreement with the precursor model proposed by Benninghoven [15].

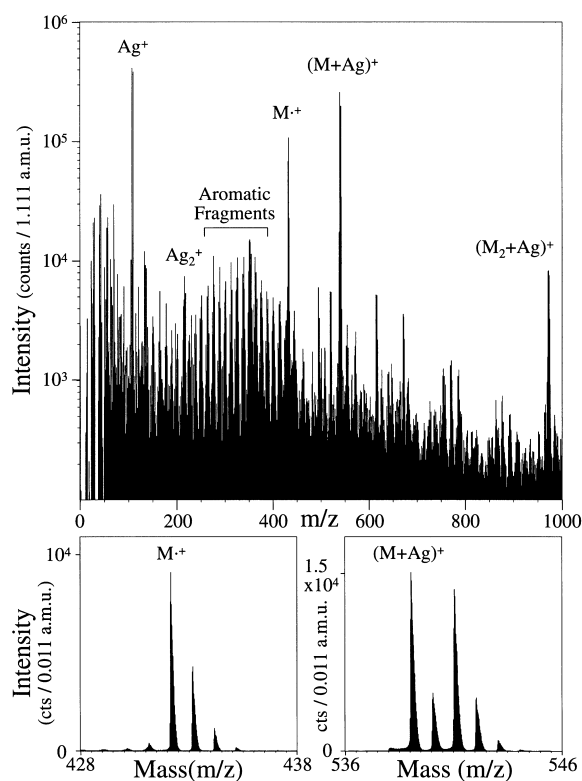


Fig. 4. Positive SI mass spectrum of TPN cast on a silver foil.

3.1.3. Dibenzanthracene

The positive ion mass spectrum of dibenzanthracene has been presented elsewhere [41,42]. The parent ion M^+ peaks at $m/z=278$ and the cationised homologues at $m/z=385$ and 387 . No dimers or trimers are observed in the spectrum. In contrast with TC and TPN, the intensity of the cationised DBA molecule is much weaker than the one of the parent ion: the ratio $I(M+Me^+)/I(M^+)$ is close to 1/3 for DBA. The weak Ag cationisation of dibenzanthracene is in agreement with data obtained by Cooks et al. with other polycyclic aromatic hydrocarbons (anthracene [6] and coronene [59]). Their explanation lies in the fact that such molecules, if they are cationised, have a greater tendency to fragment by loss of the metal ion [6].

3.1.4. Tricosenoic acid

The positive ion mass spectrum of a bilayer of tricosenoic acid deposited on a gold substrate by

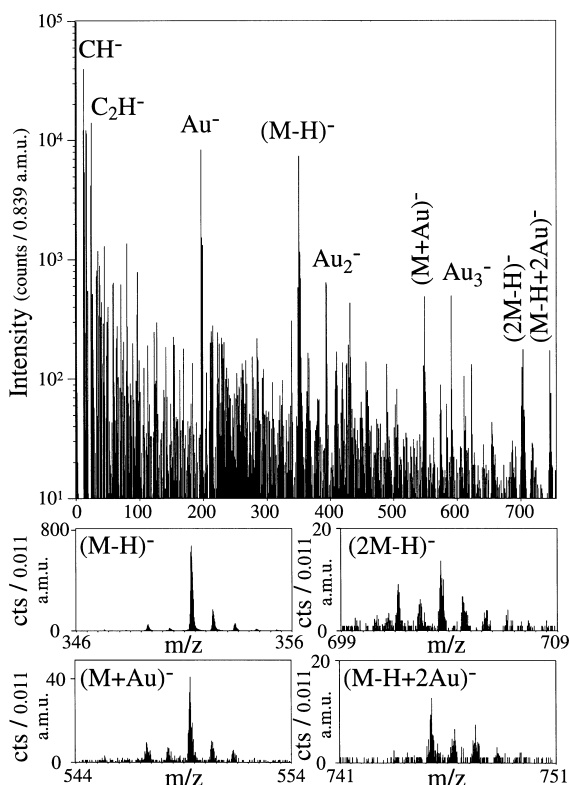


Fig. 5. Negative SI mass spectrum of a TSA bilayer transferred on a gold-metallised silicon wafer by the Langmuir–Blodgett method.

the Langmuir–Blodgett technique has been shown in a previous paper [39]. The main peaks observed above $m/z=200$ correspond to $(M-OH)^+$ ($m/z=335$), $(M+H)^+$ ($m/z=353$), $(2M-H_2O-OH)^+$ ($m/z=669$), $(2M-OH)^+$ ($m/z=687$), $(M+Au)^+$ ($m/z=549$) and $(M+H+2Au)^+$ ($m/z=747$). Note that sputtered Au-cationised dimers have been observed by Canry et al. [23,24] and simulated by Liu et al. [60] for alkanethiols self-assembled on gold, too. Although the fragmented molecule $(M-OH)^+$ dominates over the parent $(M+H)^+$, Au-cationised fragments are not observed in the spectrum. With two layers, the ratio $I(M+Au^+)/I(M+H^+)$ is equal to 9, mainly because the molecule has a tendency to fragment and produce the smaller $(M-OH)^+$ ion at the expense of the $(M+H)^+$ parent-like ion. However, this ratio is varying strongly with the layer number. In the negative spectrum (Fig. 5), the more intense

peaks above $m/z=50$ are Au^- ($m/z=197$) and $(M-H)^-$ ($m/z=351$). Weak contributions of $(M+Au)^-$ ($m/z=549$), $(2M-H)^-$ ($m/z=703$) and $(M-H+2Au)^-$ ($m/z=748$) are detected too. In sharp contrast with the positive mode, the ratio $I(M+Au^-)/I(M-H^-)$ is less than 1/10 for the same sample, due both to the much higher yield of $(M-H)^-$ and to the weak intensity of $(M+Au)^-$.

3.1.5. Polystyrene oligomers

In general, there are several series of peaks in the positive spectrum of Ag-cationised PS oligomers: (i) the fingerprint region ($0 < m/z < 200$), with fragments formed from one or two repeat units (RU) or including chain-ends (CE); (ii) the cationised oligomer distribution (centred around the polymer molecular weight); and (iii) the fragmentation region (intermediate), with a distribution of cationised fragments [8,61]. The mass distribution of the Ag-cationised oligomers is shown in Fig. 6 for PS1100. In contrast with the molecules presented before, series of cationised fragments are observed in addition to the distribution of the cationised intact oligomers. The more intense peaks of the four main series occur at $m/z=(m_M+m_{Ag}-30)$, $(m_M+m_{Ag}-58)$,

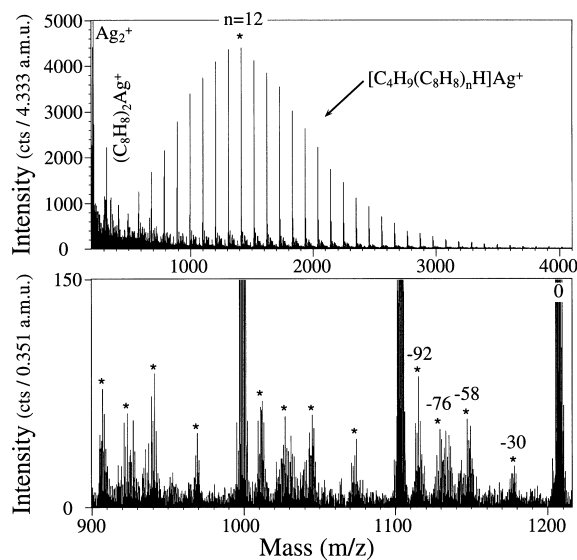


Fig. 6. Positive SI mass spectrum of PS1100 cast on a silver foil.

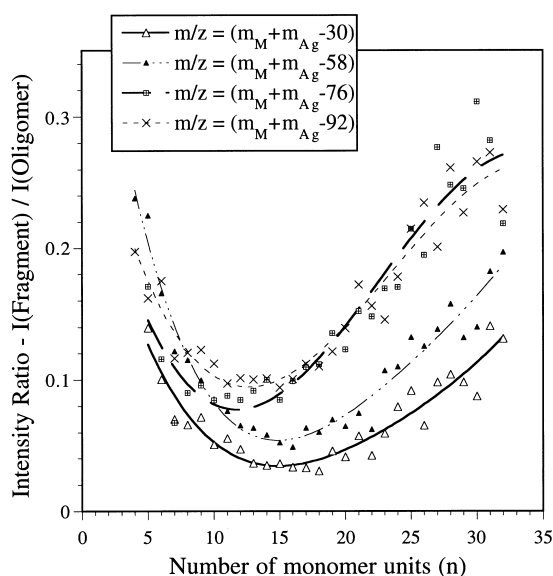


Fig. 7. Distribution of the intensity ratios (*number of cationised fragments/cationised parent*) as a function of the number of monomer units for PS1100 cast on silver.

$(m_M + m_{Ag} - 76)$ and $(m_M + m_{Ag} - 92)$, where $m_M = n \times m_{RU} + m_{CE}$ is the mass of the oligomer and m_{Ag} is the mass of silver (Fig. 6). Similar fragments were also observed for PS580 [36], PS700 and PS1700 [36]. They correspond respectively to loss of C_2H_6 , C_4H_{10} , C_6H_4 and C_7H_8 from the Ag-cationised oligomer. They are due respectively to a fragmentation at the butyl chain-end (the first two), and at the phenyl chain-end (the last two). For the fragments at $m/z = (m_M + m_{Ag} - 58)$ and $(m_M + m_{Ag} - 92)$, a loss of the corresponding (chain-end + x monomers) units cannot be excluded a priori. Smaller fragments at $m/z = 211, 315$ and 419 are attributed to the Ag-cationised monomer, dimer and trimer (without the butyl chain-end).

The intensity distribution of these four series of fragments, divided by the intensity of the cationised oligomer with the same number of repeat units, is reported in Fig. 7 as a function of the number of monomers (n) in the fragment. Distinct behaviours can be evidenced: the relative intensity of the ions produced by fragmentation of the phenyl chain-end decreases first to a minimum corresponding to 12 repeat units and then, increases

again; for the ions produced by fragmentation of the butyl chain-end, the minimum is reached later, with 15–16 repeat units. Thus, this relative variation of the fragment yield by a factor of three may explain the limited accuracy of the molecular mass determination in SIMS. The increase of fragmentation beyond the minimum can be reasonably explained by the interference between the size of the molecule and the size of the excited volume: indeed, for larger molecule sizes, the probability to exceed the size of the excited area and, consequently, the fragmentation probability, should be greater. More physically, the fraction of the molecule to which the momentum is transferred should decrease with increasing molecule size and, thus, the fraction of the energy transmitted into internal modes of vibration and rotation should increase proportionally to the size, leading to fragmentation. For PS oligomers, the probability $P(M \rightarrow X)$ to form a cationised oligomer X from a molecule M has been determined from degradation experiments by van Leyen et al. [37]. In agreement with our results, the quasi-exponential decrease of $P(M \rightarrow X)$ beyond $m/z = 2000$ was explained by the increased fragmentation of large oligomers with respect to smaller ones, as a change of the ionisation probability could be excluded.

The increase of the fragment yield below the minimum is harder to explain. In the case of fragments at $m/z = (m_M + m_{Ag} - 58)$ and $(m_M + m_{Ag} - 92)$, which show the highest fragment yield at low masses, the increase could be partially explained by the augmentation of the number of fragments resulting from the loss of the chain-end + x monomers by the parent ion. Indeed, the number of different precursors leading to the formation of a fragment with n repeat units by this reaction is $k - n$ (where k is the number of repeat units of the heaviest oligomer) and $k - n$ increases when the size of the fragment decreases. Nevertheless, the increase is observed to a lesser extent for the fragments at $m/z = (m_M + m_{Ag} - 30)$ and $(m_M + m_{Ag} - 76)$ too, indicating that this is only part of the explanation. On the other hand, the observation of a significant fraction of Ag-cationised fragments at low masses suggests that the interaction of the silver atom with the PS molecules is stronger, or that the oligomer itself is

less stable in comparison with the other compounds studied. The latter hypothesis is reinforced by the fact that purely organic parent-like ions are not observed in the spectrum. Indeed, this indicates that the ionisation of the intact molecule is less probable than the fragmentation–ionisation process leading to small fingerprint ions, probably because the energy required for the ionisation is sufficient to induce fragmentation. The ionisation by silver cations would then be an alternative, low-energy process preventing fragmentation.

3.2. Substrate effect

3.2.1. Parent-like ions

To compare the influence of the silver and copper substrates, positive SI mass spectra have been acquired from several areas of two different samples cast on silver and three samples cast on copper from three triacontane solution (0.1 , 1 and 10 mg ml^{-1}). The secondary ion yields of the parent ion and of the Me-cationised molecule are shown in Fig. 8 for the copper and silver substrates. The molecular ion yields are plotted as a function of the metal yield observed on the same area. In addition, the metal yields are normalised to the metal yield measured on etched silver and copper foils, respectively, in order to avoid the bias introduced by the different ionisation yields of the two metals. As expected, there is a positive correlation

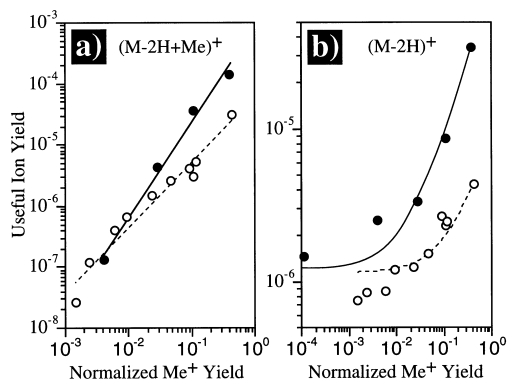


Fig. 8. Correlation between the useful yield (*number of detected secondary ions/primary ion*) of the parent-like ions and the normalised yield of the substrate ions in the case of TC cast on silver (●) and copper (○). (a) Organometallic ion; (b) parent ion.

between the yields of the cationised molecule and of the metal ion, which indicates that a thinner or less complete coverage by TC enhances the cationisation effect. The organometallic ion yields are similar for copper and silver in the case of low metal yields (less than 1% of the maximum yield), but the increase of the $(M-2H+Ag)^+$ yield is non-linear (slope > 1 in the double-log plot) whereas it remains quasi-linear for $(M-2H+Cu)^+$ (slope = 1 in the double-log plot). For the samples with the highest metal yield ($\sim 40\%$ of the maximum yield), the enhancement of the organometallic ion yield with silver is five times stronger than with copper. In the case of the molecular ion $(M-2H)^+$, a strong matrix effect due to substrate is observed too. The $(M-2H)^+$ yield, close to 10^{-6} for both substrates at high coverage, increases to 3×10^{-5} for silver and 4×10^{-6} for copper substrates at low coverage (Fig. 8b). For TC cast on silver substrates, a nearly linear correlation is obtained if the yield of $(M-2H)^+$ is plotted versus the yield of $(M-2H+Ag)^+$, instead of Ag^+ . The slope of the line indicates that $(M-2H+Ag)^+$ is 4–5 times more intense than $(M-2H)^+$ for the same samples as in Fig. 1. In the case of copper substrate, the evolution of the $(M-2H)^+$ yield is much better fitted using a power law with an exponent of $1/3$, which suggests a saturation of the enhancement when the coverage decreases.

Similar secondary ion yield measurements have been realised with three TPN samples cast on Ag, too. Figs. 9a and b show the correlations $Y(M+Ag^+)/Y(Ag^+)$ and $Y(M^+)/Y(Ag^+)$. The M^+ yield increases gradually from 1.6×10^{-5} to 1.8×10^{-3} when the coverage decreases (Fig. 9b), indicating a very strong substrate effect. The correlation $M^+/(M+Ag)^+$ is linear in this case too (not shown).

To evidence the substrate effect in the case of tricosenoic acid, samples with 0, 2, 4 and 8 LB layers were realised. In the positive mode (Fig. 10a), the influence of the substrate is limited: by the time the substrate signal increases by three orders of magnitude (from 8 LB layers to 2 LB layers), the increase of the $(M+H)^+$ and $(M-OH)^+$ yields is close to a factor of three only. The increase of the $(M-H)^-$ yield, from 8×10^{-6} to 10^{-4} , is more drastic (Fig. 10b). In fact, the

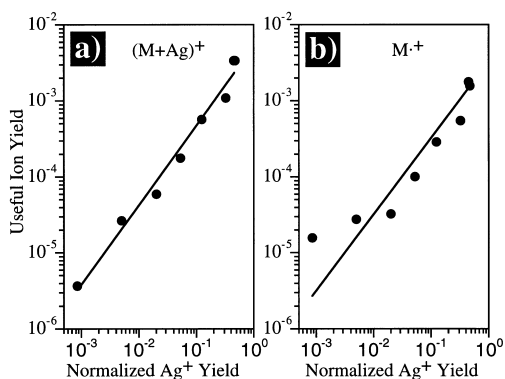


Fig. 9. Correlation between the useful yield of the parent-like ions and the normalised yield of the substrate ions in the case of TPN. (a) Organometallic ion; (b) parent ion.

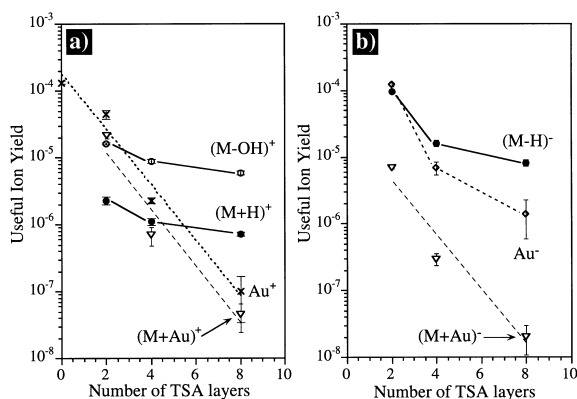


Fig. 10. Evolution of the useful yield of the substrate and parent-like ions with the number of LB layers in the case of TSA. (a) Positive ions; (b) negative ions.

very different evolutions of the two parent-like ions with increasing thickness fit rather well to the precursor model developed by Benninghoven [15], assuming that the particular interaction of the first monolayer with the substrate favours the emission of parent anions. The decay of the Au-cationised molecule intensity with increasing layer number is quasi-exponential in both positive and negative ion acquisition modes.

Concerning the different effects of the copper and silver substrates on the emission of large molecular adsorbates, the higher yields obtained with silver instead of copper are in agreement with the observations of van Leyen et al. [37]. To explain this result, a higher binding energy between

the molecule and the copper substrate has been invoked, because this must lead logically to a lower emission yield of the intact adsorbate. However, more recent measurements have shown that the interaction of hydrocarbon molecules with the copper and silver substrates was similar, leading Hagenhoff and co-workers to propose that the metal reactivity plays the dominant role [14]. In this interpretation, the probability to fragment the molecules during the deposition process increases with the metal reactivity, leading to a smaller number of intact molecules on the reactive metal with respect to the noble metal.

Another explanation is related to the nature and mass of the substrate atoms: as heavy substrate atoms may interact with several carbon atoms of the molecule, the fragmentation is reduced and intact molecular ions may be emitted more easily [25]. In addition, the spike formation probability in the substrate increases with the mass of the substrate atoms [62], which should also lead to an improved sputtering of large molecular ions. Finally, an important effect of the substrate oxidation on the ionisation probability of the adsorbate ions cannot be excluded (matrix effect) [16].

3.2.2. Fragment ions

Another interesting issue is the effect of the substrate on the extent of fragmentation of the parent molecule. The excited volume of the collision cascade (or spike), which develops mainly in the heavy metal substrate for isolated adsorbates, will gradually move towards the organic layer with increasing layer thickness. In this case, the evolution of the intensity ratios parent ions/fragment ions can be attributed to the modification of the sputtering process itself rather than to the change of the ionisation probability affecting parents and fragments in the same way. In Figs. 11a and b, the intensity of the quasi-molecular ion $(M-2H)^+$ is divided by the intensity of two smaller characteristic fragments of TC: $C_7H_{13}^+$ and $(M-4H)^+$. The evolution of this ratio indicates a different behaviour for copper and silver supports. For TC cast on copper, the development of the cascade in the substrate (low coverage) does not significantly change the ratio parent ions/fragment ions: $Y(M-2H^+)/Y(C_7H_{13}^+)$ remains nearly constant

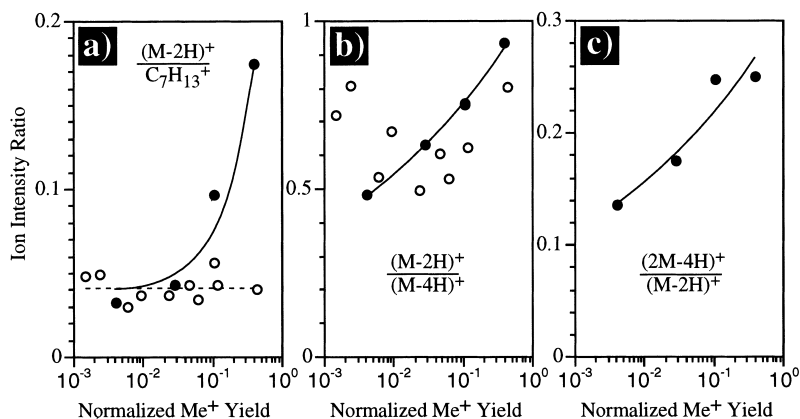


Fig. 11. Correlation between the intensity ratios: (a) $(M-2H)^+/C_7H_{13}^+$; (b) $(M-2H)^+/(M-4H)^+$; (c) $(2M-4H)^+/(M-2H)^+$ and the normalised yield of the substrate ions in the case of TC cast on silver (●) and copper (○).

whatever the coverage and $Y(M-2H^+)/Y(M-4H^+)$ remains in the range 0.5–0.9 without any correlation with the substrate coverage. In contrast, the two ratios increase significantly with the silver ion yield for TC cast on silver: $Y(M-2H^+)/Y(C_7H_{13}^+)$ increases by a factor of four and $Y(M-2H^+)/Y(M-4H^+)$ by a factor of two when $Y(Ag^+)$ increases from 5×10^{-5} to 5×10^{-3} . Moreover, the ratio dimer/monomer (Fig. 11c) increases by a factor of two when the Ag^+ yield reaches 10% of its maximum value.

For TPN cast on silver, a qualitatively similar increase is observed with the intensity ratio parent ion/fragment ion. This shows unambiguously that the use of a silver substrate improves selectively the emission of intact parent-like ions for TC and TPN.

Again, the different behaviours observed for copper and silver might be due to the higher reactivity of copper, reducing the number of intact molecules on the surface, or to the different energy deposition in the surface region, which is directly related to the nature of the substrate.

Two important conclusions can be drawn from the experiments reported in Sections 3.1 and 3.2: (i) The cationisation of organic molecules with transition metal atoms of the substrate occurs for all the considered systems. The efficiency of the cationisation process varies from low (DBA/Ag) to very high (TPN/Ag; TPN/Au). Organometallic anions are observed with gold substrates exclu-

sively. (ii) The substrate effect is drastic for very dilute molecule solutions cast on metals. In that case, both the fragment ion, the parent ion and the cationised molecule intensities are enhanced. With silver substrates, the enhancement is stronger for large parent-like ions than for small fragment ions.

3.3. Kinetic energy and velocity distributions

In this section, we will focus on the kinetic energy and velocity distributions of the cationised molecules in relation to the three formation hypotheses described in the introduction.

Figs. 12a–d show the KED of the metal, of the parent ion and of the Me-cationised molecule for TC, TPN, DBA and TSA, respectively. The shape of the metal ion KEDs indicates clearly the collisional nature of the sputtering process [47]. The maxima of the parent-like ion KEDs are in the region 0–2 eV for TC and TSA, and 2–4 eV for TPN and DBA. In addition, the KEDs of TPN and DBA exhibit high energy tails expanding beyond 10 eV, which suggest a collisional emission process, too (Fig. 13). Table 2 summarises the features of the distributions presented in Fig. 12 (maximum position, FWHM and width at 10 per cent of the maximum, slope of the high energy tail), with an estimation of the reproducibility for TC, TPN and DBA. For TC and TSA, the width of the measured KEDs is close to the theoretical

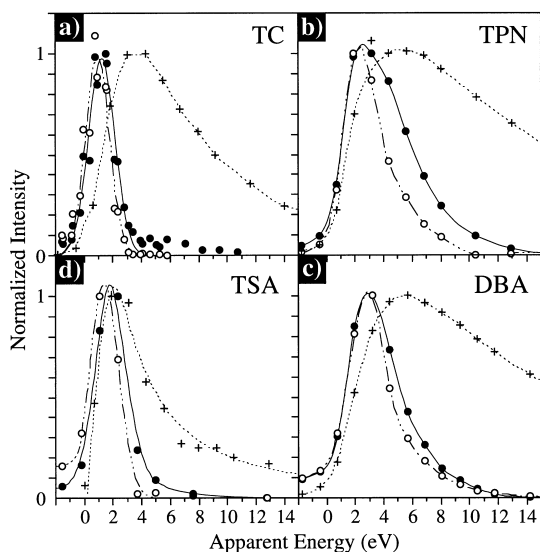


Fig. 12. Positive part of the kinetic energy distribution of the parent ion (\circ), the cationised-parent ion (\bullet) and the atomic metal ion ($+$) for: (a) TC; (b) TPN; (c) DBA cast on silver; (d) 2 LB layers of TSA on gold.

resolution fixed by the energy slit (1.5 eV). This artefact might partially mask the real shape of the distribution. Table 2 confirms that, on average, aliphatic hydrocarbon parent ions and Me-cationised molecules are emitted with less kinetic energy than aromatics (TC and TSA compared to TPN and DBA), supporting the idea that polyaromatic ions are more resistant against fragmentation than long alkyl chains. This is particularly evident when looking at the full widths at 10 per cent of the maximum. For TPN and DBA, the slope of the high energy tails is close to the predictions of Urbassek (E^{-5}) [63], Hoogerbrugge et al. ($E^{-4.5}$) [64,65] and Haring et al. ($E^{-4.5}$) [66] for the uncorrelated double collision process. In the case of TC, one may notice a change of slope in the high energy tail of the Me-cationised molecule KED beyond 5 eV (Fig. 13), which is not observed in the parent ion KED. After that point, the slope of the high energy tail is close to the one of the parent-like ions of TPN and DBA (Table 2). The change of slope might suggest the contribution of two emission mechanisms, with different characteristic mean energies. Presumably, the high energy contribution would then be collisional.

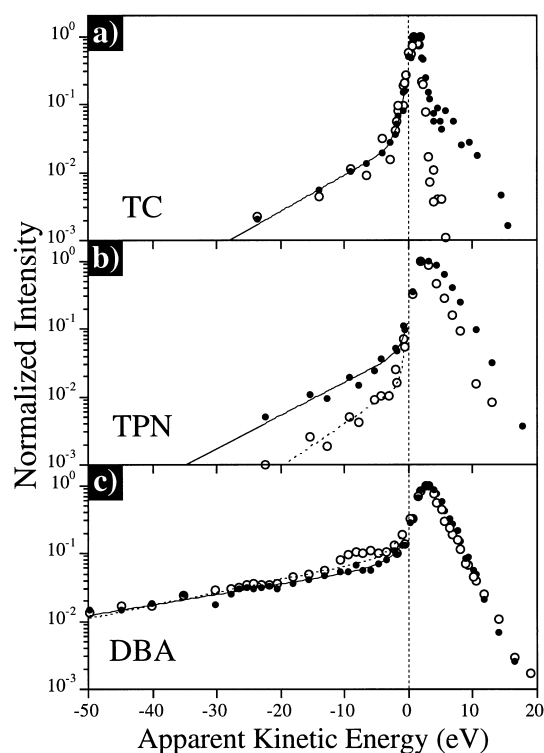


Fig. 13. Negative part of the kinetic energy distribution of the parent ion (\circ) and the cationised-parent ion (\bullet) for: (a) TC; (b) TPN; (c) DBA cast on silver.

In contrast with previous observations [15,31], the difference between the parent and cationised parent KEDs, indicated by the shift of the maximum and/or by the width of the distribution is significant, too. In general, the KEDs of the Me-cationised molecules are broader and peak at a higher energy than those of the characteristic fragment and parents. This effect is particularly marked for TPN. In this respect, it should be noted that, as the KED measurement is realised in parallel for all secondary ions, the error indicated in Table 2 is certainly over-estimated when comparing the KEDs of ions sputtered from the same sample. For example, it is clear from Fig. 12 that beyond the maximum of the parent ion KED, *each point* in the distribution of the Me-cationised molecule is systematically higher than the corresponding point in the parent energy spectrum, and this is true for all the samples analysed. In Table 2, the characteristic values corresponding to larger

Table 2

Characteristic values of the KEDs for parent-like ions sputtered from TC, TPN, DBA and TSA

	Maximum (eV)	FWHM (eV)	FW 10% (eV)	High energy tail
TC	Estimated error ^a : ±0.1	Estimated error ^a : ±0.2	Estimated error ^a : ±0.2	
(M–2H) ⁺	0.9	2.1	4.0	$E^{-5.1}$
(M–2H+Ag) ⁺	1.3	2.5	4.7	$E^{-4.2}$
(M–3H+2Ag) ⁺	1.2	2.6	5.4	– ^b
(2M–4H) ⁺	1.2	2.8	5.5	– ^b
(2M–4H+Ag) ⁺	1.5	2.9	6.5 (±0.3)	– ^b
TPN	Error: ±0.1	Error: ±0.3	Error: ±0.3	
M ⁺	2.1	3.2	7.7	$E^{-4.4}$
(M+Ag) ⁺	2.6	5.2	10.6	$E^{-4.3}$
DBA	Error: ±0.1	Error: ±0.3	Error: ±0.3	
M ⁺	2.8	3.4	9.0	$E^{-4.3}$
(M+Ag) ⁺	2.9	4.2	9.8	$E^{-4.3}$
TSA				
(M+H) ⁺	1.3	2.2	4.2	– ^b
(M+Ag) ⁺	1.8	2.4	5.3	– ^b

^a The error has been estimated on the basis of the KED measurements realised with four TC samples, three TPN samples and three DBA samples.

^b The intensity at high energy is very weak.

aggregates (Me_xM_y^+) sputtered from TC indicate a substantial broadening of the KEDs with increasing molecule size.

The direct emission hypothesis is difficult to test on the basis of KEDs of the molecules considered before because it requires important assumptions about the sputtering event (linear collision cascade, simultaneous uncorrelated or correlated motion of the substrate atoms, etc.). In the case of the linear collision cascade, assuming that the difference of binding energy is not drastic, the kinetic energy transmitted to the departing organometallic should decrease with the size of the molecule [38,39,67,68], which is not observed. Moreover, in the case of triacontane, the KEDs of the dimer and cationised dimer are broader than those of the monomer and cationised monomer (Table 2). On the other hand, the amount of fragmentation should strongly depend on the Me–M bond, and thus, on the considered molecule, which does not allow a direct comparison between different parent ion KEDs. Nevertheless, in the case of TC, one should expect a lower energy threshold for fragmentation for the dimer than for the monomer, if the two molecules are weakly bound in the dimer. From that viewpoint, the increase of the FWHM with the molecule size, at least for TC monomers

and dimers, is in contradiction with a direct emission based on the interaction with a single cascade atom (linear collision cascade [69]), although these values do not allow us to choose between the three hypothesis considered in the introduction. To verify more correctly the effect of the molecule size on the kinetic energy, one should compare very similar molecules with different sizes. This will be done with polystyrene oligomers in the following.

In contrast, the metastable decay of large ions either in the surface region or in the field region would have clear consequences on the kinetic energy and velocity distributions of their daughters. If the dissociation occurs in the surface region, the velocity distributions of the daughters should be similar, and their kinetic energy should be proportional to their mass. If it occurs in the field region, the daughter ions will be detected with a negative apparent energy in the KED [51], as explained in the introduction. Fig. 13 shows the negative part of the KED for TC, TPN and DBA, corresponding to metastable decay reactions occurring in the acceleration section of the spectrometer. The importance of the metastable decay process is obvious for DBA. Fig. 13a and c indicate that the fraction of parents and cationised parents produced in the vacuum are comparable in the

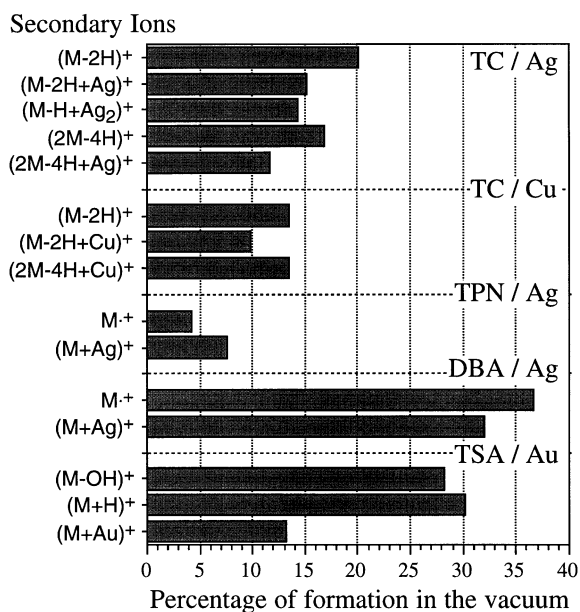


Fig. 14. Percentage of ion formation in the acceleration section of the spectrometer for the parent-like ions of TC, TPN, DBA and TSA on various substrates.

cases of TC and DBA. Unexpectedly, for TPN (Fig. 13b), the ion production in the vacuum is even larger for the cationised-parent ion than for the parent itself. To determine quantitatively the relative fractions of ions formed in the vacuum, the negative part of the KEDs (Fig. 13) has been integrated. The metastable fractions are indicated in Fig. 14 for the ions of interest in this study. The accuracy of these fractions is limited by the error made in the calibration of the zero energy, by the error due to the convolution of the KEDs with 1.5 eV passband, but the most important limitation may be related to the amount of metastable ions appearing in the positive part of the distributions: for instance, a parent with 5 eV initial kinetic energy undergoing fragmentation when the energy brought by the field does not exceed some eV would lose only a few eV during the dissociation and the apparent energy of the daughter might remain positive, but closer to the zero than the apparent energy of an unfragmented parent with the same initial energy [44]. Therefore, the metastable fraction is probably underestimated. Nevertheless, these limiting factors should affect

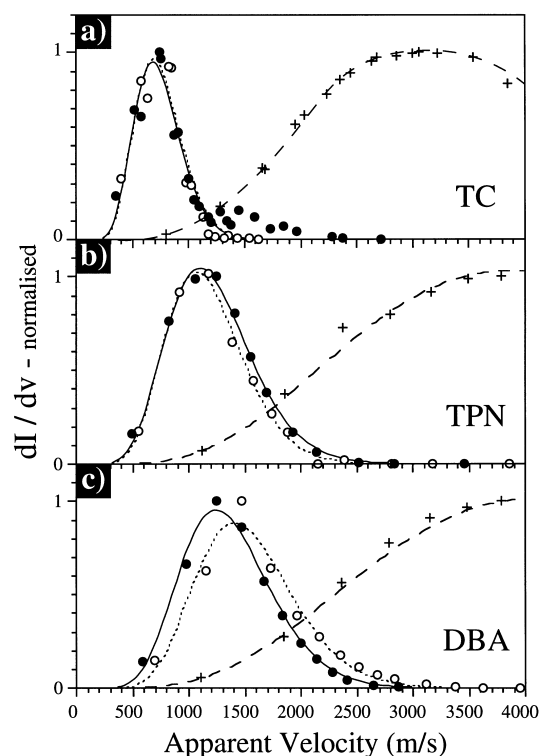


Fig. 15. Velocity distributions derived from the kinetic energy of the parent ion (\circ), the cationised-parent ion (\bullet) and the atomic metal ion (\times) for: (a) TC; (b) TPN; (c) DBA cast on silver.

all the ions in a similar way, allowing us to compare the different systems. In Fig. 14, the highest values are observed for DBA and TSA (30%), the lowest for TPN (5%). TC shows intermediate values. In the case of TSA, the percentage of formation in the vacuum is much lower for the organometallic. As the fraction of ions produced in the electric field is significant for both the organometallic and the organic parent-like ions of each compound, one may assume that the parents for these metastable decay reactions are larger aggregates of the kind M_x^+ and $M_xMe_y^+$.

The velocity distributions of the silver ion, of the parent ion and of the Me-cationised molecule, deduced from the KEDs by the equation $dI/dv = dI/dE \times dE/dv$, are displayed in Fig. 15a–c for TC, TPN and DBA. In the case of TPN and TC, the parent and cationised parent have similar distributions, which is expected if these ions are formed

by the decay of the same $M_xMe_y^+$ aggregates before entering the field region. In this hypothesis, the parents could be the cationised dimers or trimers. The increase of the FWHM of the KEDs with increasing fragment mass for TC is consistent with this explanation, too (Table 2). If the parent ions M^+ were simply produced by the metastable decay of a given fraction of the organometallic $(M+Ag)^+$, in agreement with the linear correlation observed between the M^+ and $(M+Ag)^+$ yields, the identical velocity distributions of the two ions would mean that the internal energy, responsible for the fragmentation, is not correlated at all with the kinetic energy of the parent, which is not usually the case [38, 39, 68, 70]. Indeed, when the internal and kinetic energies are correlated, the internal energy dependent fragmentation of the parent induces a depletion of the high energy (or high velocity) tail of the distributions. In addition, this could not explain the negative energy tail of the organometallic ion KEDs in Fig. 13. It is striking to see that the two compounds for which the velocity distributions are similar (TC and TPN) are those which exhibit the lowest fraction of ions formed by metastable decay in the electric field. In contrast, this fraction is very high for DBA although the velocity distributions of the parent and cationised parent are slightly different. This lack of correlation between two effects which should be both aspects of the same process seems to indicate that metastable decay reactions are not the reason for the similar velocity distributions in Fig. 15a and b, except if the dissociation rates are so different that these reactions occur mainly in the “selvedge” region for TC and TPN. Nevertheless, it is clear from Fig. 14 that unimolecular dissociation reactions constitute an important formation mechanism for all the ions considered.

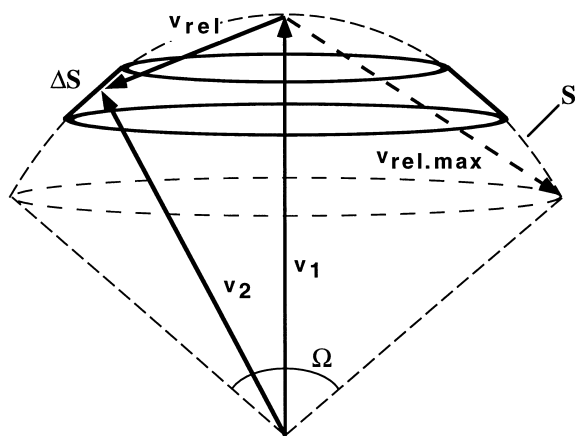
Particularly broad organometallic ion distributions have been measured and simulated by Garrison too [25], for $C_6H_6Ni^+$ sputtered from benzene adsorbed on Nickel. Garrison’s simulations are explained by the association of the ejected metal atom and organic molecule in the surface region, provided that they have the same velocity and move in parallel directions. In her case, the C_6H_6 and Ni distributions peak at the same energy. As C_6H_6 and Ni have similar masses, their velocity

distributions are similar too, which should be reflected by the velocity distribution of the organometallic. Thus, the KED of the organometallic should peak at higher energy than both the KEDs of C_6H_6 and Ni. Experimentally, she observed that Ni^+ and $C_6H_6Ni^+$ had very similar KEDs, except for the high energy tail above 10 eV. To reconcile simulations and experiments, she introduced a correction accounting for the force applied on the ejected ions as a result of the polarisation of electrons in the metal (image force) [25]. However, there is an important difference with our measurements: Fig. 12 shows that the KED of the metal is always much broader and peaks at higher energy than the KED of the parent ion, which was not true for the benzene–nickel system.

To test the recombination hypothesis, the velocity distribution of an hypothetical organometallic formed by the recombination of a molecule with a metal ion having the same velocity can be calculated from the experimental distributions of the parent ion and of the metal ion. However, an important assumption is made by using the distribution of M^+ instead of M . The organometallic ion distribution can be determined with the following equation:

$$N(M+Ag; v_f) = N(M; v_1) \times N(Ag; v_2) \times P(v_{rel}), \quad (1)$$

where $N(X; v)$ are the intensities of the different ejected particles, $P(v_{rel})$ is a recombination probability and $v_{rel} = v_2 - v_1$. The relative orientations of the vectors v_1 and v_2 (Scheme 2) are very important because they fix the value of the relevant parameter v_{rel} for the determination of the recombination probability $P(v_{rel})$. For instance, ions travelling in near-parallel directions will have a different recombination probability than ions travelling in opposite directions. To take into account the orientations of the vectors v_1 and v_2 , a series of distributions has been calculated for different values of v_{rel} from 0 to $v_{rel,max}$, where $v_{rel,max}$ is the maximum relative velocity below which the association of the two particles may occur. This velocity corresponds to an energy threshold $E_{rel,max}$ above which the association is no longer possible, e.g. the relative energy is too high and other phenomena take place (frag-



Scheme 2. Geometric description of the vectors and angles considered for the calculation of the organometallic ion velocities.

mentation, reorganisation [38,39]). In a first approximation, the experimental distributions $N(X; v)$ have been used instead of the angle-resolved velocity distributions $N(X; \mathbf{v})$. For each value of v_{rel} , the final velocity of the assembly has been calculated assuming that the collision is totally inelastic [$(m_1 + m_2)v_f = m_1v_1 + m_2v_2$]. The resulting distributions are expressed by the relation

$$N(M + \text{Ag}, v_f) \div N(M; v) \times N(\text{Ag}; v) \times f(\Omega), \quad (2)$$

where $f(\Omega)$ is the probability to have the velocity vector of the second particle in the solid angle defined by v_1 and $v_1 + v_{\text{rel.max}}$, which decreases with increasing v , inducing a depletion of the $(M + \text{Ag})^+$ distributions at high velocity. The distributions corresponding to different v_{rel} are finally weighted by the corresponding fraction of solid angle $\Delta\Omega = \Delta S/v^2$ and summed. In the calculation, the threshold velocity $v_{\text{rel.max}}$ is taken as a fitting parameter. It must be noted that the use of the simple factor $f(\Omega)$ is an important approximation allowing us to overcome our lack of knowledge about the angular distributions and angle-resolved velocity distributions of the particles. Using $f(\Omega)$, we consider implicitly that the angle-resolved velocity distributions are identical, which is of course a rough approximation.

The result of the calculation is shown in Fig. 16a for TPN. The best value of $E_{\text{rel.max}}$ is 5 eV. It is interesting to note that a good fit at high velocity is obtained with the lowest value of $E_{\text{rel.max}}$ too

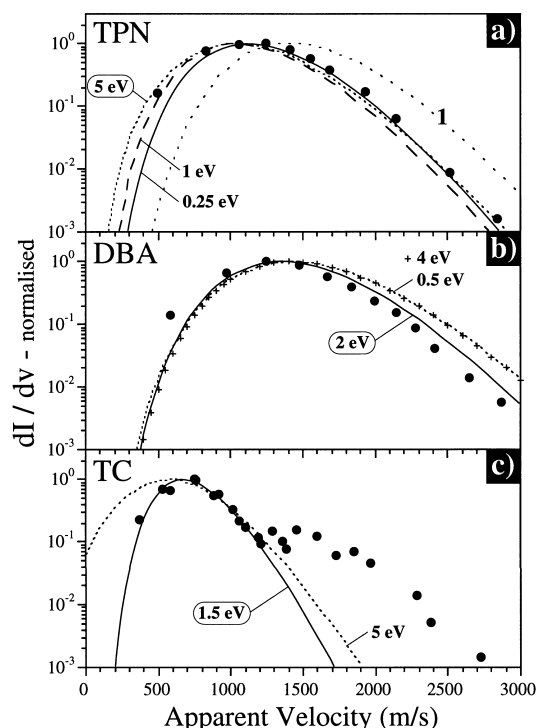


Fig. 16. Comparison between the calculated velocities (—, · · ·) and the distributions derived from the kinetic energy of the cationised-parent ion (●) for: (a) TC; (b) TPN; (c) DBA cast on silver. See text for details of the calculation.

(0.25 eV), intermediate values leading to worse fits. For comparison purpose, a hypothetical distribution $N(M; v) \times N(\text{Ag}; v)$, neglecting the relative orientations of the velocity vectors, would correspond to curve 1 in Fig. 16a. In the case of DBA, the organometallic ion velocities calculated by this simple treatment do not agree so well with the experimental distributions (Fig. 16b). The best agreement corresponds to $E_{\text{rel.max}} = 2$ eV, whereas lower and higher values lead to worse fits. Although the calculated curves fit the shape of the measured distribution, they match only approximately. For TC, the model may account for the first part of the experimental distribution, with $E_{\text{rel.max}} = 1.5$ eV (Fig. 16c). A higher value of the fitting parameter $E_{\text{rel.max}}$ (5 eV) does certainly not lead to a better agreement with the whole distribution.

In summary, this model based on simple arguments tends to show that the formation of

$(M+Ag)^+$ by the recombination of M and Ag^+ in the selvedge is realistic, from the viewpoint of the KEDs. The best values of $E_{rel,max}$ are of the same order of magnitude as the binding energies in the molecule, which corresponds rather well to the idea that a relative kinetic energy which is higher than this threshold would prevent the association of the two particles by inducing the fragmentation of the parent molecule M . In the case of TPN, the shape of the distribution is satisfactorily modelled, but the high intensity measured for the organometallic ion (Table 1) is poorly compatible with the small fraction of the silver ion distribution corresponding to the main part of the parent ion distribution in Fig. 15. Indeed, to explain the absolute intensity measured at the maximum of the $(M+Ag)^+$ velocity distribution (1000 m s^{-1}), one would require, at least, a one order of magnitude greater initial Ag^+ intensity at this velocity, before recombination. Such a high recombination probability (more than 90%) is not realistic. In addition, this process would induce a pronounced depletion in the low-energy part of the observed Ag^+ distributions, which is not the case: the shape of the silver ion KEDs measured on etched silver with or without TPN are similar. The even higher $I(M+Me^+)/I(Me^+)$ ratio obtained with pristine TPN cast on gold reinforces this argument (Table 1). Therefore, recombination in the selvedge is certainly not the major formation process for metal-cationised TPN molecules. This argument is not valid in the case of DBA, for which the cationised molecule intensity is very low. Finally, the recombination hypothesis is reasonable in the case of TC, but another emission mechanism is required to explain the high velocity part of the distribution.

The KEDs of Ag^+ , Ag_2^+ and Ag_3^+ sputtered from PS1100 cast on silver are presented in Fig. 17a. The maxima are located at 6.0, 3.4 and 2.2 eV, respectively, and the slopes of the high energy tails are equal to $E^{-2.0}$, $E^{-2.7}$ and $E^{-3.6}$. The narrowing of the KED with increasing cluster size is in agreement with the literature [16]. The KEDs of the cationised macromolecules are all rather broad ($4.0 \text{ eV} < 6.0 \text{ eV}$) and exhibit a high energy tail (Fig. 17b). The maximum of the KEDs is in the range 2.5 to 3.5 eV. The slope of the high

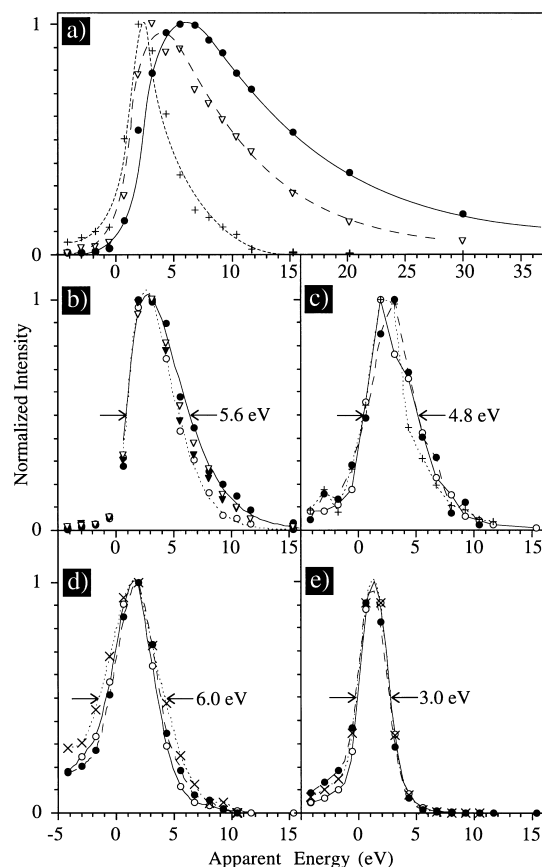


Fig. 17. Kinetic energy distribution of secondary ions sputtered from a PS1100-covered silver substrate: (a) Ag^+ (\bullet), Ag_2^+ (∇), Ag_3^+ ($+$); (b) $[C_4H_9(C_8H_8)_nH]Ag^+$ for $n=4$ (\circ), $n=5$ (\blacktriangledown), $n=6$ (∇), $n=12$ (\bullet); (c) $[C_4H_9(C_8H_8)_3C_9H_9]Ag^+$ ($+$), $[C_4H_9(C_8H_8)_4C_9H_9]Ag^+$ (\circ), $[C_8H_7(C_8H_8)_5H]Ag^+$ (\bullet); (d) $[(C_8H_8)_n]Ag^+$ for $n=1$ (\circ), $n=2$ (\bullet), $n=3$ (\times); (e) $C_7H_7^+$ (\circ), $C_9H_5^+$ (\bullet), $C_{15}H_{13}^+$ (\times).

energy tail is close to $E^{-3.5}$ for large cationised macromolecules ($m/z=1309$; 1413) and becomes steeper (E^{-5}) for smaller molecules ($m/z=581$; 685). Preliminary results concerning these KEDs were presented elsewhere [4,71], and the same features were found with PS700. These distributions look very similar to the one of the cationised molecule of TPN (see Fig. 12b and Table 2), which is the closest to PS from the viewpoint of the chemical structure. The energy of the maximum, as well as the high-energy dependence of these distributions support the collisional character of the emission process. However, in contrast with

smaller molecules, metastable decay reactions account for less than 2.5% of the total integrated intensity of these ion distributions. Fig. 17c shows the energy spectra of some cationised fragments belonging to the series at $m/z = (m_M + m_{Ag} - 58)$ and $(m_M + m_{Ag} - 92)$. The curve shapes are rather ill-defined because the yield of these fragments, sampled by the 1.5 eV slit for the KED measurement, is very weak. For the same reason, the KEDs of fragments at $m/z = (m_M + m_{Ag} - 30)$ and $(m_M + m_{Ag} - 76)$ could not be satisfactorily measured. Nevertheless, there is no significant difference between the KEDs of these fragments and those of the cationised parents, except for negative apparent energies, where the fragments keep a significant intensity. For instance, the fractions of these fragment ions produced in the electric field are 12% for $[\text{C}_4\text{H}_9(\text{C}_8\text{H}_8)_4\text{C}_9\text{H}_9]\text{Ag}^+$ ($m/z = 697$) and 14% for $[\text{C}_8\text{H}_7(\text{C}_8\text{H}_8)_5\text{H}]\text{Ag}^+$ ($m/z = 731$). In contrast, the KEDs of smaller fragments (Fig. 17d), $[(\text{C}_8\text{H}_8)_n]\text{Ag}^+$ ($1 \leq n \leq 3$), with similar FWHMs (4.3 eV < 5.6 eV) than the cationised oligomers, exhibit very different shapes and peak at a lower energy (approximately 1.5 eV). Their high energy tail is depleted and, in parallel, the ion fraction produced in the vacuum is very large, as shown by the important intensity observed for negative apparent energies. The depletion of the high energy tail is also partially due to unimolecular dissociation occurring in a region of the field close to the surface. As mentioned before, this is due to the fact that the daughters of parents decaying when their kinetic energy gained in the field does not exceed some eV (or tenths of eV) will keep a lower, but positive, apparent kinetic energy. The fractions of these ions corresponding to the negative energy tails are 28% for $[(\text{C}_8\text{H}_8)]\text{Ag}^+$ ($m/z = 211$), 26% for $[(\text{C}_8\text{H}_8)_2]\text{Ag}^+$ ($m/z = 315$) and 31% for $[(\text{C}_8\text{H}_8)_3]\text{Ag}^+$ ($m/z = 419$). Finally, Fig. 17e shows the energy spectra of several fingerprint ions of PS: C_7H_7^+ , C_9H_9^+ and $\text{C}_{15}\text{H}_{13}^+$. They are all very narrow (2.5 eV < 3.0 eV) and peak between 1 and 1.5 eV [41,42].

To get more information about the emission process, it is interesting to compare the FWHMs of the cationised oligomers with different sizes. Fig. 18a shows that the variation of the FWHM with the mass of the molecule follows a power

law ($y = 1.62x^{0.16}$). This increase of the kinetic energy corresponds to a decrease of the mean velocity (Fig. 18b). As suspected from the weak contribution of unimolecular dissociation in the electric field, the different velocity distributions of Fig. 18b confirm that metastable decay is certainly not the predominant ion formation mechanism for silver-cationised PS oligomers. Other arguments support this interpretation: (i) The size of even one single oligomer can be large with respect to the size of the excited area [74]. (ii) With the sample preparation, the macrochains are disentangled and, thus, probably separated on the surface (cationisation is more efficient with very dilute solution); at least, there is no reason for two molecules to be sufficiently strongly bound together or with the substrate atoms (crystallinity, etc.). (iii) There is no peak in the mass spectrum indicating the association of two macromolecules.

Considered in the frame of the precursor model, the weak increase of the mean kinetic energy with the molecule size is in disagreement with an emission process based on single atom collisions, where the preformed cluster ($\text{M} + \text{Ag}$) is recoiled by a substrate silver atom. As mentioned before, one should observe a decrease of the mean kinetic energy in that case, because the energy fraction transferred in the vibration and rotation modes increases with the molecule size, leading to fragmentation [38,39]. However, this evolution cannot exclude a multiple collision process, where, for instance, the number of substrate atoms involved increases with the molecule size, with a subsequent increase of the energy transmitted to the molecule in a correlated way.

To have a qualitative idea about the shape of the curve describing the kinetic energy of the molecule as a function of its size in the multiple collision hypothesis, one can consider a hemispherical molecule of radius R deposited on the metal substrate. In a first approximation, we assume that the excited area is larger than the molecule and that the interaction is undertaken with the atoms of the molecule which are in contact with the substrate. Then, the part of the molecule interacting directly with the recoiling substrate atoms is limited to an annular of height h and the molecule can be divided into two sub-units, the first one (m_1) being set in motion by the correlated

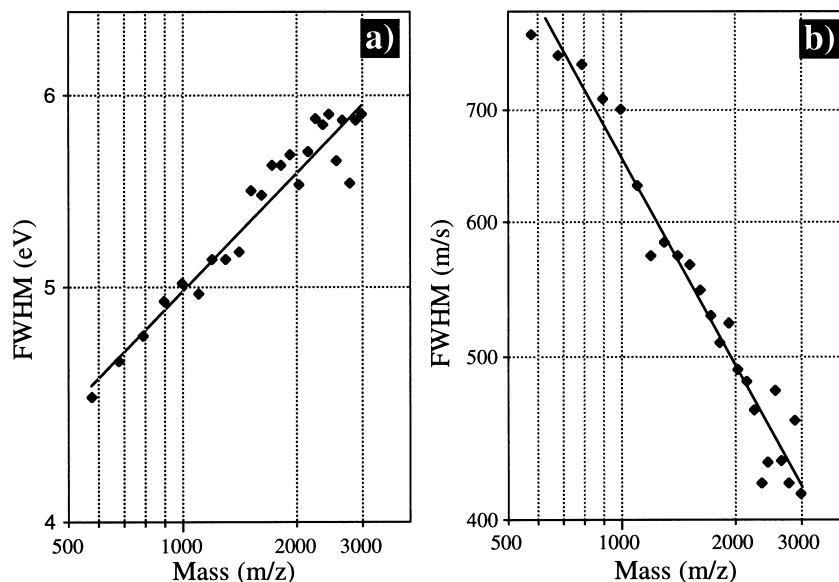


Fig. 18. FWHM of the kinetic energy (a) and derived velocity distributions (b) for PS1100-cationised oligomers.

momentum and the second one (m_2) being initially at rest. Treating the two sub-units as rigid bodies, we can roughly approximate the kinetic energy of the departing molecule by the equation $E_k = m_1/(m_1 + m_2)E$ [38,39,68], where E_k is the kinetic energy of the molecule, m_1 and m_2 are the masses of the sub-units and E is the total energy corresponding to the momentum transferred by the substrate atoms. (i) If R is smaller than h , the whole molecule is directly set in motion by the correlated impact and $E_k = E$. In addition, E should be proportional to the size of the interface between the molecule and the substrate, i.e. to R^2 . An alternative and more realistic case is constituted by adsorbates lying completely flat on the substrate: the area occupied by the molecules is then proportional to their mass (m_M) and a linear relationship should be observed between the kinetic energy and the mass of the molecules. (ii) If R is greater than h , m_1 and E remain proportional to R^2 whereas the total molecule mass is proportional to R^3 , and thus, E_k should be proportional to $R^{4/3}$, i.e. to $m_M^{1/3}$. This qualitative explanation accounts for the increase of the kinetic energy with mass in the case of correlated momentum transfer. In contrast, in the case of a single atom impact, m_1 and E would be constant, leading to a decrease

of E_k with the mass of the molecule. A similar trend has been observed for small fragment ions ($m/z < 100$) sputtered from organic and polymer thin films [38–42,44,46] and simulated by molecular dynamics calculations [26]. In this explanation, the binding energy of the molecule to the substrate has been completely neglected. For cyclosporin adsorbed on silver, a desorption energy of 1.32 eV has been obtained from temperature programmed SIMS experiments [73]. In fact, the successful emission of large organic adsorbates anchored to the surface by a number of weak bonds, as it is the case for hydrocarbons, is in favour of a multiple collision process too.

In the recombination hypothesis, the decrease of the $(M + Ag)^+$ velocity with the molecule size (Fig. 18b) should be due to a parallel decrease of the neutral molecule velocity, as the distribution of Ag^+ does not change. As indicated by the calculations described for smaller molecules, this velocity decrease should also correspond to a soft increase of the kinetic energy of the neutral molecule with mass. For the same reasons as before, this suggests that, even in the recombination hypothesis, the emission of the neutral molecule would need the combined motion of several underlying substrate molecules.

The analysis of the parent-like ion KEDs leads to the following conclusions: (i) In general, the emission is less energetic for organic parent ions than for metal cationised molecules. (ii) Molecules containing aromatic rings (TPN, DBA, PS) have a higher mean kinetic energy than purely aliphatic compounds (TC, TSA) and a pronounced high energy tail, indicating collisional sputtering. In the case of aliphatics, the 1.5 eV energy resolution of the slit does not allow us to conclude. Nevertheless, the change of slope in the high energy tail of the KED of $(M-2H+Ag)^+$ sputtered from TC suggests a collisional contribution, too (Figs. 13 and 16). (iii) Metastable decay reactions contribute strongly to the parent-like ion emission, especially for DBA. The metastable contribution is much lower for TPN and PS. (iv) The direct emission by a single substrate atom may not explain the observed distributions; instead, the combined action of several substrate atoms may account for the broadening of the KEDs with increasing molecule size. (v) On the strict basis of the KEDs, the recombination of the silver ions with the sputtered neutral molecules is realistic too.

3.4. Ion beam degradation studies

In order to learn more about the emission mechanisms of the parent and cationised-parent ions, degradation studies were realised for TPN and TC. Three different degradation experiments have been realised for TPN: (i) degradation of a “thick” layer of TPN cast on silicon (more concentrated solution, see experimental section); (ii) degradation of a “thick” layer of TPN cast on silver; and (iii) degradation of a “thin” layer of TPN cast on silver (more dilute solution). For TPN cast on silicon, no substrate ion was detected, indicating a defect-free layer (50 Å thickness or more [75]). The same deposition conditions on silver give different results: silver and silver-cationised molecules are present in the spectrum with weak intensities, indicating either an incomplete coverage or a non-uniform thickness of the layer. This may be explained by the large roughness of the silver foils in contrast to the flat, polished silicon wafers: the solution mainly fills the valleys and very few TPN is deposited on the tops [76].

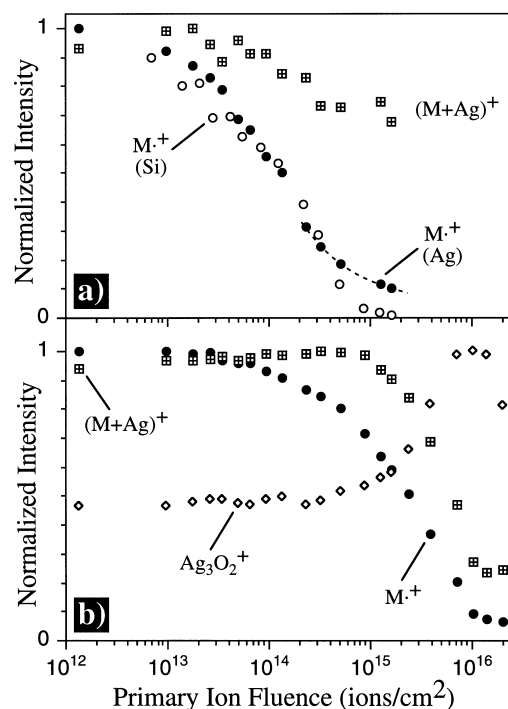


Fig. 19. Evolution of the substrate and parent-like ion intensities as a function of the primary ion fluence for TPN: (a) concentrated solution cast on silicon ($M^+(Si)$) and silver ($M^+(Ag)$ and $(M+Ag)^+$); (b) dilute solution (see text for details).

With this interpretation, the cationisation regions are expected to be the silver tops emerging from the TPN film. In Fig. 19a, one can see that the decay of the parent (M^+) ion intensity is very similar for the “thick” samples, half of the initial intensity being reached with a fluence close to 10^{14} ions cm^{-2} ($F_{1/2}$). Nevertheless, a difference occurs beyond 3×10^{14} ions cm^{-2} : while the intensity falls down quickly for the TPN/Si system, it tends to stabilise for the TPN/Ag system (from 4×10^{14} to 2×10^{15} ions cm^{-2}). Unexpectedly, the $(M+Ag)^+$ signal decreases very weakly in the range 10^{12} – 10^{15} ions cm^{-2} . The similar evolutions of the M^+ signal for the two substrates indicates that the contribution of the cationisation regions to this ion intensity is weak in the “thick” sample. The fact that the degradation is faster in the thick areas (M^+) than in the cationisation regions ($M+Ag^+$) might be related to different modes of

energy dissipation in the different zones, but we will see that another explanation may be invoked.

When a very dilute solution is used (Fig. 19b), the decay of the M^+ signal is much slower ($F_{1/2} = 10^{15}$ ions cm^{-2}). In that sample, the initial yields of M^+ and $(M+Ag)^+$ are both two orders of magnitude higher in comparison with the first experiment. These very high initial yields of M^+ and $(M+Ag)^+$ (above 10^{-3} , see Fig. 9) indicate a predominant substrate effect and show that the M^+ signal originates mostly from the same regions of the sample as the cationisation. Again, the degradation rate of the parent ion is faster than those of the cationised molecule and dimer. The increase of the $Ag_3O_2^+$ signal with the parallel decay of the cationised molecule intensity beyond 10^{15} ions cm^{-2} indicates that the organic layer has been sputtered and that the substrate surface oxide layer has been reached. The decay of the Ag^+ signal when the oxide layer is sputtered (not shown) is most probably due to the ionisation probability change accompanying deoxygenation of the substrate [16].

Another explanation for the very slow decay of the characteristic ion intensities with primary ion fluence is related to the migration of pristine material from areas which are not sampled by the primary ion beam [77]. This is suggested by the spectrum acquired on the same area of the thin sample and without additional sputter time, but one hour after the last measurement reported in Fig. 19b. In this spectrum, the $(M+Ag)^+$ intensity is two times stronger, and the M^+ intensity is two times weaker than the initial intensities reported in Fig. 19b. In contrast, the silver oxide signal has not changed. The drastic change of the measured yields shows that the surface is again partly covered by pristine TPN molecules. To investigate the mechanism, another sample was sputtered with a fluence of 1.8×10^{15} ions cm^{-2} on a $190 \times 190 \mu m^2$ area and then surface chemical mappings were realised at regular time intervals to observe the evolution of the surface composition. The chosen sample area was particularly rough. Fig. 20 shows the evolution of the $(M+Ag)^+$ signal as a function of time, after sputtering. Five minutes after sputtering, the remaining signal comes mainly from scratches in the sample. It is

reduced by a factor of six with respect to the initial signal. This already shows that, in addition to the total primary ion fluence, the fluence deposition rate plays an important role in the degradation of TPN (in this case: one high-fluence continuous bombardment + one static analysis). Indeed, for a similar total ion fluence (1.8×10^{15} ions cm^{-2}), but with a different bombardment regime allowing relaxation of the surface during the experiment (Fig. 19b), the decay of $(M+Ag)^+$ has just begun. With time, the intensity increases around the scratches and from the borders of the sputtered area, suggesting that the pristine material migrates from the holes and borders to the whole analysed area. For the same experiment, the intensity variation of several secondary ions of interest is reported in Fig. 21. First, the reduction of the $Ag_3O_2^+$ intensity by a factor of seven indicates that the oxide layer has been almost completely sputtered. In addition, the remaining signal comes from the borders of the analysed area, i.e. from the edges of the “crater”, where the sputtering conditions are ill-defined. It is important to note that this oxide signal does not change any more after sputtering. With time, the $(M+Ag)^+$ signal slowly recovers its initial intensity, although the surface oxide layer is definitely absent. As expected from the preceding experiment, the first and last images in Fig. 20 show that the $(M+Ag)^+$ intensity may be even larger on the covered area of metallic silver than on silver oxide. The M^+ intensity increases much more slowly, and the ratio $I(M^+)/I(M+Ag^+)$ decreases from 1/2 before sputtering to 1/10 after sputtering. In fact, it is an indication that the M^+ parent ion intensity is strongly altered by the change of ionisation probability due to the sputtering of the oxide layer. On the other hand, the evolution of $(M+Ag)^+$ seems mostly determined by the change of the surface structure: the association of the molecule with a silver atom is favoured when the substrate surface is a metal instead of an oxide. The variation of the Ag^+ signal is interesting too: five minutes after sputtering, the Ag^+ intensity is strongly reduced because of the drastic change of the ionisation probability due to the oxide layer sputtering. After that, it increases slowly with time, which can be explained by a new increase of the ionisation

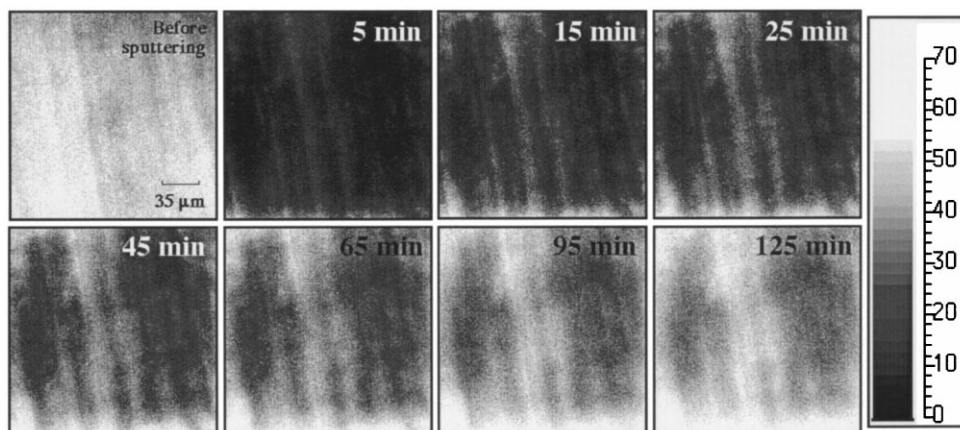


Fig. 20. Chemical mappings of the $(M+Ag)^+$ ions sputtered from a dilute TPN solution cast on a silver foil, before sputter cleaning and at regular time intervals after sputter cleaning with a primary ion fluence of 1.8×10^{15} ions cm^{-2} .

probability related to the organic “matrix” constituted by the pristine TPN migrating on the freshly sputter cleaned surface. Recent evidences of such matrix effects have been reported by Egbers et al. [73].

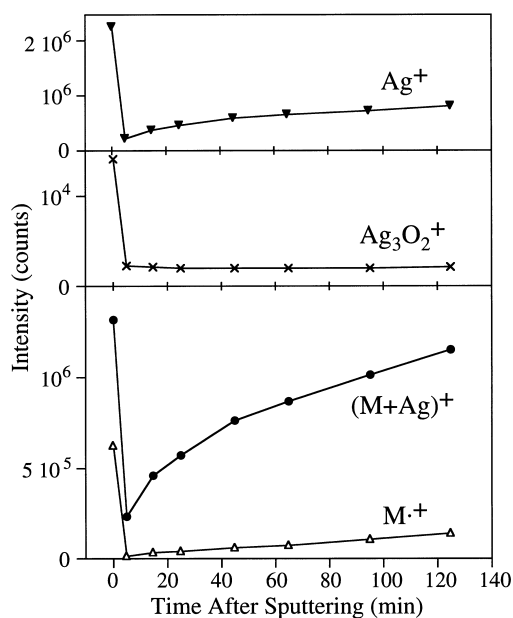


Fig. 21. Evolution of the intensity of the substrate and parent-like ions sputtered from a dilute TPN solution cast on a silver foil, before sputter cleaning and at regular time intervals after sputter cleaning with a primary ion fluence of 1.8×10^{15} ions cm^{-2} (same experiment as in Fig. 20).

All these results confirm the migration of fresh material on the sputtered surface. As a consequence, the influence of the degradation regime (continuous bombardment alternated with analysis periods) on the results obtained with TPN is marked, and may explain the high cumulated fluence needed for the degradation (Fig. 19b).

For TC, a sample cast from the more dilute solution was sputtered in the same way (Fig. 22). In this case, the very high initial yields of silver, of the parent-like ion and of the cationised molecule (above 10^{-4} ; see Fig. 8) show that the emission of the large molecular ions is dominated by the substrate effect. The degradation is much

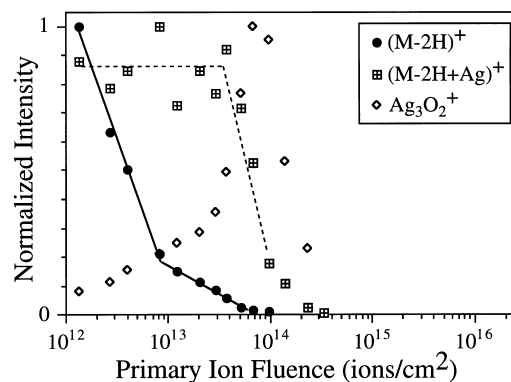


Fig. 22. Evolution of the substrate and parent-like ion intensities as a function of the primary ion fluence for a dilute TC solution cast on silver (see experimental section).

faster than with TPN for both $(M-2H)^+$ ($F_{1/2}=4 \times 10^{12}$ ions cm^{-2}) and $(M-2H+Ag)^+$ ($F_{1/2}=7 \times 10^{13}$ ions cm^{-2}). The intensity of $(M-2H+Ag)^+$ is reduced by a factor of 200 with a fluence of 3.3×10^{14} ions cm^{-2} . Again, the decay of the organometallic ion intensity corresponds to the complete sputtering of the organic layer, as indicated by the Ag_2O_3 profile. A spectrum acquired on the same area but one hour after the last data point indicates that the $(M-2H+Ag)^+$ intensity remains 40 times weaker than the initial signal and that there is no trace of the parent ions any more, showing that migration plays a minor role in their degradation profiles.

Concerning the emission processes, the different evolutions of the organic and organometallic parent-like ions is a very important point because it excludes a formation process of M^+ based only on the metastable decay of $(M+Ag)^+$ or $M_x\text{Ag}_y^+$. Indeed, in that case, the ratio $I(M^+)/I(M+Ag^+)$ should remain rather constant because the nature of an isolated sputtering event realised in the static analysis mode should not change drastically with increasing induced damage, in terms of kinetic and internal energy transmitted to the ejected particles. Therefore, metastable decay reactions may not be the explanation for the similar velocity distributions described in Section 3.3. On the other hand, the different evolutions of the parent ion and silver-cationised molecule in Figs. 19 and 22 do not exclude the precursor hypothesis, because the modification of the surface chemistry could also affect the different ion fractions.

The fact that the $(M+Ag)^+$ variation is not correlated with the Ag^+ variation in Fig. 21 is in disagreement with an emission process based on the recombination in the selvedge: to explain the $(M+Ag)^+$ increase in this frame, one should also invoke an important change of the neutral molecule yield. In addition, the $(M+Ag)^+$ yield is even greater than the Ag^+ yield at the end of the experiment (Fig. 21), which would mean that more than 50% of the Ag^+ ions react with sputtered neutral molecules to produce organometallic ions. Once more, such a high recombination probability is unrealistic. Instead, the emission of an organometallic complex preformed at the surface might

explain the experimental observations reasonably: (i) the sputtering of the surface oxide layer leads to a decrease of the ionisation probabilities explaining the behaviour of Ag^+ and M^+ until the end of the experiment; and (ii) the change of the Ag bonding state, from covalent to metallic, and the parallel increase of the silver atomic fraction at the surface favours the formation of the $(M+Ag)$ complex.

In summary, ion beam degradation experiments bring new arguments indicating that beside metastable decay and, possibly, recombination processes, a dominant contribution of direct emission must be postulated for the sputtering of parent-like ions from TC and TPN.

4. Discussion and conclusions

Several questions arise concerning the emission of large molecular ions and clusters: (i) Can large molecular ions be sputtered by a single cascade recoil atom or do they need the simultaneous interaction with several substrate atoms to be emitted? In the particular case of cationisation, (ii) is the formation of organometallic ions due to direct emission, to metastable decay of larger aggregates or to recombination in the selvedge? (iii) What is the exact role of the substrate in the emission process? To address these issues, a critical review of the models must be done within the frame defined by the experimental results obtained in this paper and in the literature.

Concerning the first question, there are recent evidences based on computer simulations (Ar 5 keV on Cu) by Betz and Husinsky [47,78] for an emission process involving the correlated motion of several atoms in the collision cascade and leading to the sputtering of clusters formed by neighbouring surface atoms. In that simulation, a protrusion is formed around the primary ion impact point and clusters are emitted from the rim of the protrusion, indicating that the expansion of the surface is responsible for the highly correlated momentum transfer [78]. The simulations also show that cluster emission is a late event. In addition, Winograd and co-workers [79] pointed out several years ago that, for collisions below,

say, 10 eV, binary collisions are improbable because the nuclear stopping cross-sections are such that every substrate atom “touches” its neighbours. An emission process based on spikes in the matrix has also been invoked by Sundqvist [80] and by Wong and Röllgen [29] to explain the emission of large molecular ions, and the spike formation probability under keV ion bombardment has been calculated by Bitensky [62]. On the other hand, multiple collisions leading to particle desorption have been postulated and simulated by Garrison’s group to explain the emission of intact benzene [25,26] and, more recently, biphenyl molecules [81] adsorbed on metals (respectively Ti and Cu). In our experiments with DBA, TPN and mainly PS, the broad kinetic energy distributions of the cationised oligomers also showed that the direct emission of these macromolecules by the interaction with a single cascade atom is improbable: to transfer 5 eV or more in the translational mode of such a large molecule by a localised impact requires a much more energetic collision. Such a violent momentum transfer to a highly localised part of the molecule should lead to the fragmentation of the molecule instead of its emission, especially with a weaker metal–organic bond inside the molecule. The increased mean kinetic energy of TC dimers as compared to monomers, and of large PS oligomers as compared to smaller ones also suggest an emission process based on multiple correlated collisions. Indeed, the parallel increase of the energy transferred in the internal and vibrational mode by a localised impact should even lead to a more efficient fragmentation in the case of the fragile TC dimers and silver-cationised PS oligomers. Thus, our findings add to the body of experiments supporting the model of multiple correlated collisions to depict the emission of large molecular adsorbates.

We have shown in previous papers that unimolecular dissociation of positive ions in the vacuum, especially the loss of H and H₂, is an important mechanism of ion formation for hydrocarbon secondary ions [41,42,44,46]. Similar metastable losses of metal atoms from metal clusters were experimentally demonstrated earlier by Dzhemilev et al. [51]. More generally, metastable decay reactions are probable (and observed) events in SIMS

[17,82], as well as in PDMS [83,84]. As exemplified in Ref. [85], the literature shows that metastable decay reactions play an important role in the very last step of the emission process, favouring the more stable clusters. However, there is no reason to believe that the initial, regular size distribution of the cluster ions is the result of metastable decay reactions. For hydrocarbons cast on silver (especially for DBA) and unsaturated fatty acid deposited on gold, our results indicate that a substantial fraction of parent-like ions is produced by metastable decay of large M_xMe_y⁺ aggregates in the vacuum. Beside direct emission processes, unimolecular dissociation constitutes then a complex channel leading to the delayed formation of these ions.

Although there are general arguments for a direct emission process of large molecular ions based on multiple correlated collisions, in the particular case of metal cationisation, it is more difficult to determine whether the association of the organic molecule with the metal atom is realised before, during or after the emission itself.

With a simple model, we have indicated that an emission process based on the recombination of the sputtered molecule with a substrate atom (or ion), as proposed several years ago by Garrison and Winograd [25,26,79], is compatible with the shape of the measured KEDs (see Section 3.3). However, the respective (M+Me)⁺ and Me⁺ ion yields measured for TPN cast on silver and gold show that recombination cannot be the major process. In addition, the calculated distribution of recombined organometallics does not explain the high-energy part of the (M–2H+Ag)⁺ distributions in the case of TC. The same treatment cannot be applied for PS oligomers because the parent ions are not observed, and therefore, the KEDs of the oligomers are not available.

On the other hand, our results do not exclude the possibility for an organometallic complex to be directly emitted by the concerted action of several substrate atoms. As argued before, the weakness of the organometallic bonding [6] would even reinforce the hypothesis of correlated momentum transfer, which would be the only means to sputter them without further fragmentation. For the same reason, it is probable that the surviving

complexes originate from a region where the deposited energy per substrate atom is low, and rather far away from the primary impact point. This fits nicely with the view of Betz in which the cluster emission is a rather late, low energy (per atom) event. In this hypothesis, the greater kinetic energy observed for Me-cationised molecules with respect to parent ions can be explained by the additional kinetic energy brought by the heavy substrate cation accompanying the parent molecule with the same velocity. Moreover, the similar velocity distributions of the parent ions and Me-cationised molecules indicate that the momentum transfer is directly proportional to the mass, in agreement with our explanation for molecules lying flat on the substrate (Section 3.3).

The drastic influence of the substrate has been demonstrated in Section 3.2 for TC and TPN. As quoted before, it has been shown by Bitsensky for thin organic films deposited on various substrates that the probability of spike formation in the substrate leading to a shock wave and, thus, to the emission of unfragmented organic molecules is significant even for keV ion bombardment [62]. Moreover, this probability increases with the mass of the substrate atoms due to higher energy loss, which enlightens the effect of the substrate on the sputtering of large molecules itself. For hydrocarbon molecules cast on a silver oxide surface, the increase of the organic film thickness leads to a decrease of the parent ion yield due to the change of the ionisation probability. In this frame, this effect would be reinforced by the decrease of the spike formation probability, which may explain the much larger substrate effect observed in our measurements for large molecular ions than for small fragment ions ($C_2H_3^+$). Another argument in favour of the increase of the molecule sputtering yield for heavy substrates has been given by Garrison [25], the larger size of the substrate atoms allowing a simultaneous interaction with several carbon atoms of the molecule. In this way, the momentum is shared between the interacting carbon atoms and the fragmentation probability is reduced. However, this argument may not account for the evolution of the kinetic energy with the size of the molecule (Section 3.3). From the degradation experiments realised with TPN

(Section 3.4), the drastic variation of the ratio $I(M^+)/I(M+Ag^+)$ for oxide and metallic surfaces cannot be explained solely by the variation of the ionisation probability related to the electronic properties of the substrate. In our opinion, the increase of the $(M+Ag)^+$ yield for the metal surface, in contrast with the parallel decay of the M^+ yield, indicates a real augmentation of the formation probability of the $(M+Ag)$ complex.

Finally, in the cationisation of hydrocarbons, results have been obtained with molecules containing aromatic rings or, at least, unsaturation [30–32]. This is valid in our experiments with DBA and TPN, and, to a certain extent, with triacontane too, which supports the explanation based on the metal–ligand bonding theory briefly presented in the introduction. In this respect, the similarity of the organometallic compounds formed with copper, silver and gold is consistent with their similar properties of transition metals (Ib group). However, to explain the peak cluster around $m/z = 527$ in the TC spectrum, one has to admit that a certain fraction of saturated $(M+Ag)^+$ is present. Thus, this view of the M–Ag bonding involving the π -electron system of the hydrocarbon, valid for transition metals, is probably too simple and σ -bonding might play a role too.

In conclusion, our results point to a collisional mechanism of secondary ion emission to explain the keV ion induced sputtering of both parent ions and Me-cationised molecules from large adsorbates on metal substrates. The observations are consistent with a model based on the correlated momentum transfer due to the nearly simultaneous interaction of several substrate atoms with the organic molecule. By this way, small amounts of the cascade energy might be distributed to several atoms in the molecule(s), preventing fragmentation, even in the case of large molecular aggregates. Due to the number of atoms involved, the sum of the energy fractions transferred to the molecule (or aggregate) would explain the measured kinetic energies. Finally, when large aggregates are sputtered with an excess of internal energy, they may undergo fragmentation during their time-of-flight to the detector, which leads to the delayed production of smaller parent-like ions. More simula-

tion results are needed to check the validity of this proposed mechanism.

Acknowledgements

The authors wish to thank B.G. Segda and S. Errkiba for their contribution in the measurements and data processing and Dr. L. Langer for the preparation of the tricosenoic acid LB films. Dr. B.W. Schueler from Phi-Evans is gratefully acknowledged for stimulating comments and discussions. This work and A. Delcorte are supported by the “Action de Recherche Concertée” (94/99-173) of the “Communauté Française de Belgique”. The ToF-SIMS equipment was acquired with the support of the “Région Wallonne” and “FRFC – Loterie Nationale” of Belgium.

References

- [1] S.J. Pachuta, R.J. Cooks, *Chem. Rev.* 87 (1987) 647.
- [2] P.A. Demirev, *Mass Spectrom. Rev.* 14 (1995) 279.
- [3] G.J. Leggett, J.C. Vickerman, *Int. J. Mass Spectrom. Ion Proc.* 122 (1992) 281.
- [4] K. Wien, *Nucl. Instrum. Methods B* 131 (1997) 38.
- [5] H. Grade, N. Winograd, R.G. Cooks, *J. Am. Chem. Soc.* 99 (1977) 7725.
- [6] H. Grade, R.G. Cooks, *J. Am. Chem. Soc.* 100 (1978) 5615.
- [7] I.V. Bletsos, D.M. Hercules, D. vanLeyen, A. Benninghoven, *Macromolecules* 20 (1987) 407.
- [8] I.V. Bletsos, D.M. Hercules, D. van Leyen, B. Hagenhoff, E. Niehuis, A. Benninghoven, *Anal. Chem.* 63 (1991) 1953.
- [9] P.A. Zimmerman, D.M. Hercules, *Appl. Spectrosc.* 47 (1993) 1545.
- [10] A. Benninghoven, B. Hagenhoff, E. Niehuis, *Anal. Chem.* 65 (1993) 630A.
- [11] A. Benninghoven, *Surf. Sci.* 299/300 (1994) 246.
- [12] K. Xu, A. Proctor, D.M. Hercules, *Mikrochim. Acta* 122 (1996) 1.
- [13] A.J. Nicola, D.C. Muddiman, D.M. Hercules, *J. Am. Soc. Mass Spectrom.* 7 (1996) 467.
- [14] B. Hagenhoff, in: *Wiley Static SIMS Library*, Wiley, New York, 1996, p. 39.
- [15] A. Benninghoven, in: A. Benninghoven (Ed.), *Ion Formation from Organic Solids*, Springer Series in Chemical Physics 25, Springer-Verlag, Berlin, 1983, p. 77.
- [16] A. Benninghoven, F.G. Rüdener, H.W. Werner, *Secondary Ion Mass Spectrometry*, Wiley, New York, 1987, p. 699.
- [17] B. Schueler, R. Beavis, W. Ens, D.E. Main, X. Tang, K.G. Standing, *Int. J. Mass Spectrom. Ion Proc.* 92 (1989) 185.
- [18] A. Brown, J.C. Vickerman, *Surf. Sci.* 117 (1982) 154.
- [19] A. Brown, J.C. Vickerman, *Surf. Sci.* 124 (1983) 267.
- [20] A. Brown, J.C. Vickerman, *Surf. Sci.* 151 (1985) 319.
- [21] B.H. Sakakini, N. Dunhill, C. Harendt, B. Steeples, J.C. Vickerman, *Surf. Sci.* 189–190 (1987) 211.
- [22] B.H. Sakakini, I.A. Ransley, C.F. Oduoza, J.C. Vickerman, M.A. Chesters, *Surf. Sci.* 271 (1992) 227.
- [23] J.-C. Canry, J.C. Vickerman, in: A. Benninghoven, B. Hagenhoff, H.W. Werner (Eds.), *SIMS X Proceedings*, Wiley, New York, 1997, p. 623.
- [24] J.-C. Canry, J.C. Vickerman, in: H.J. Mathieu, B. Reihl, D. Briggs (Eds.), *ECASIA95 Proceedings*, Wiley, New York, 1996, p. 903.
- [25] B. Garrison, *J. Am. Chem. Soc.* 104 (1982) 6211.
- [26] B. Garrison, *Int. J. Mass Spectrom. Ion Phys.* 53 (1983) 243.
- [27] D. Holtkamp, M. Kempken, P. Klüsener, A. Benninghoven, *J. Vac. Sci. Technol. A* 5 (1987) 2912.
- [28] K.L. Busch, B.H. Hsu, Y.-X. Xie, R.G. Cooks, *Anal. Chem.* 55 (1983) 1157.
- [29] S.S. Wong, F.W. Röllgen, *Nucl. Instrum. Methods B* 14 (1986) 436.
- [30] J.H. Wandass, J.A. Gardella, *J. Am. Chem. Soc.* 107 (1985) 6192.
- [31] N. Hebert, J.C. Blais, G. Bolbach, J. Inchaouh, *Int. J. Mass Spectrom. Ion Proc.* 70 (1986) 45.
- [32] D. Pleul, F. Simon, H.-J. Jacobasch, *Fresenius J. Anal. Chem.* 357 (1997) 684.
- [33] C. Elschenbroich, A. Salzer, *Organometallics, A Concise Introduction*, VCH, Weinheim, 1989.
- [34] R.W. Linton, M.P. Mawn, A.M. Belu, J.M. DeSimone, M.O. Hunt Jr., Y.Z. Menciloglu, H.G. Cramer, A. Benninghoven, *Surf. Interface Anal.* 20 (1993) 991.
- [35] C. Simon, Thesis, Metz, 1996.
- [36] I. Fallais, Undergraduate Thesis, Louvain-La-Neuve, 1995.
- [37] D. van Leyen, B. Hagenhoff, E. Niehuis, A. Benninghoven, I.V. Bletsos, D.M. Hercules, *J. Vac. Sci. Technol. A* 7 (1989) 1790.
- [38] A. Delcorte, P. Bertrand, *Nucl. Instrum. Methods B* 115 (1996) 246.
- [39] A. Delcorte, P. Bertrand, *Nucl. Instrum. Methods B* 117 (1996) 235.
- [40] A. Delcorte, P. Bertrand, in: A. Benninghoven, B. Hagenhoff, H.W. Werner (Eds.), *SIMS X Proceedings*, Wiley, New York, 1997, p. 731.
- [41] A. Delcorte, B.G. Segda, P. Bertrand, *Surf. Sci.* 381 (1997) 18.
- [42] A. Delcorte, B.G. Segda, P. Bertrand, *Surf. Sci.* 389 (1997) 393.
- [44] A. Delcorte, P. Bertrand, *Nucl. Instrum. Methods B* 135 (1998) 430.

- [46] A. Delcorte, P. Bertrand, in: R. Lareau, G. Gillen (Eds.), SIMS XI Proceedings, Wiley, New York, 1998, p. 447.
- [47] G. Betz, K. Wien, *Int. J. Mass Spectrom. Ion Proc.* 140 (1994) 1.
- [48] R.M. Papaléo, G. Brinkmalm, D. Fenyő, J. Eriksson, H.-F. Kammer, P. Demirev, P. Hakansson, B.U.R. Sundqvist, *Nucl. Instrum. Methods B* 91 (1994) 667.
- [49] R.M. Papaléo, P. Demirev, J. Eriksson, P. Hakansson, B.U.R. Sundqvist, *Phys. Rev. B* 54 (1996) 3173.
- [50] R.A. Zubarev, U. Abeywarna, P. Hakansson, P. Demirev, B.U.R. Sundqvist, *Rapid Commun. Mass Spectrom.* 10 (1996) 1966.
- [51] N.K. Dzhemilev, A.M. Goldenberg, I.V. Veriovin, S.V. Verkhoturov, *Nucl. Instrum. Methods B* 114 (1996) 245.
- [52] D. Briggs, M.J. Hearn, *Vacuum* 36 (1986) 1005.
- [53] G.J. Leggett, J.C. Vickerman, *Appl. Surf. Sci.* 55 (1992) 105.
- [54] A. Delcorte, L.T. Weng, P. Bertrand, *Nucl. Instrum. Methods B* 100 (1995) 213.
- [55] B.W. Schueler, *Microsc. Microanal. Microstruct.* 3 (1992) 119.
- [56] B.W. Schueler, private communication.
- [57] A. Spool, presented at SIMS XI, Orlando, September 1997.
- [59] R.J. Day, S.E. Unger, R.G. Cooks, *Anal. Chem.* 52 (1980) 557A.
- [60] K.S.S. Liu, J.C. Vickerman, B.J. Garrison, in: R. Lareau, G. Gillen (Eds.), SIMS XI Proceedings, Wiley, New York, 1998, p. 443.
- [61] P. Bertrand, L.T. Weng, in: D. Brune, R. Hellborg, H.J. Whitlow, O. Hunderi (Eds.), *Surface Characterization, a User's Sourcebook*, Wiley, New York, 1997, p. 344.
- [62] I.S. Bitsensky, *Nucl. Instrum. Methods B* 83 (1993) 110.
- [63] H.M. Urbassek, *Nucl. Instrum. Methods B* 18 (1987) 587.
- [64] R. Hoogerbrugge, P.G. Kistemaker, *Nucl. Instrum. Methods B* 21 (1987) 37.
- [65] R. Hoogerbrugge, W.J. Van Der Zande, P.G. Kistemaker, *Nucl. Instrum. Methods B* 76 (1987) 239.
- [66] R.A. Haring, H.E. Rosendaal, P.C. Zalm, *Nucl. Instrum. Methods B* 28 (1987) 205.
- [67] K. Snowdon, *Nucl. Instrum. Methods B* 9 (1985) 132.
- [68] P. Sigmund, H.M. Urbassek, D. Matragrano, *Nucl. Instrum. Methods B* 14 (1986) 495.
- [69] P. Sigmund, in: R. Behrisch (Ed.), *Sputtering by Particle Bombardment I*, Springer Verlag, Berlin, 1981, p. 9.
- [70] R.A. Haring, R. Pedrys, D.J. Oostra, A. Haring, A.E. De Vries, *Nucl. Instrum. Methods B* 5 (1984) 483.
- [71] A. Delcorte, P. Bertrand, presented at IISC 11, Wangerooge, September 1996.
- [73] G. Egbers, K. Hackling, A. Benninghoven, in: R. Lareau, G. Gillen (Eds.), SIMS XI Proceedings, Wiley, New York, 1998, p. 549.
- [74] D.M. Hercules, *J. Mol. Struct.* 292 (1993) 49.
- [75] A. Delcorte, P. Bertrand, X. Arys, A. Jonas, E. Wischerhoff, B. Mayer, A. Laschewsky, *Surf. Sci.* 366 (1996) 149.
- [76] D.C. Muddiman, A.H. Brockman, A. Proctor, M. Houalla, D.M. Hercules, *J. Phys. Chem.* 98 (1994) 11570.
- [77] M. Deimel, H. Rulle, V. Liebing, A. Benninghoven, in: A. Benninghoven, B. Hagenhoff, H.W. Werner (Eds.), SIMS X Proceedings, Wiley, New York, 1997, p. 755.
- [78] G. Betz, W. Husinsky, *Nucl. Instrum. Methods B* 102 (1995) 281.
- [79] N. Winograd, B. Garrison, in: A.W. Czanderna, D.M. Hercules (Eds.), *Ion Spectroscopies for Surface Analysis*, Plenum Press, New York, 1991, p. 58.
- [80] B.U.R. Sundqvist, *Nucl. Instrum. Methods B* 48 (1990) 517.
- [81] R. Zaric, B. Pearson, K.D. Krantzman, B.J. Garrison, in: R. Lareau, G. Gillen (Eds.), SIMS XI Proceedings, Wiley, New York, 1998, p. 601.
- [82] H. Feld, A. Leute, D. Rading, A. Benninghoven, M.P. Chiarelli, D.M. Hercules, *Anal. Chem.* 65 (1993) 1947.
- [83] X. Tang, W. Ens, N. Poppe-Schriemer, K.G. Standing, in: K.G. Standing, W. Ens (Eds.), *Methods and Mechanisms for Producing Ions from Large Molecules*, Plenum Press, New York, 1991, p. 139.
- [84] R.A. Zubarev, Thesis, Uppsala, 1997.
- [85] H.M. Urbassek, W.O. Hoffer, in: P. Sigmund (Ed.), *Fundamental Processes in Sputtering of Atoms and Molecules*, *Mat. Phys. Medd.* 43, Copenhagen, 1993, p. 97.